Fine Scale Hydrologic Model Implementation and Fine-Scale/Macro-Scale Model Inter-comparison Study

Pablo Carrasco [2]
Alan F. Hamlet [1,2]

[1] Center for Science of the Earth System, Climate Impacts Group, University of Washington
[2] Dept of Civil and Environmental Engineering, University of Washington

1. Introduction and Background

In climate change assessments, simulations of hydrologic variables such as snowpack, streamflow, soil moisture, and stream temperature are potentially sensitive to the resolution and physics of the hydrologic model used in the assessment. The Columbia Basin Climate Change Scenarios Project (CBCCSP) uses the Variable Infiltration Capacity (VIC) macro-scale hydrologic model (Liang *et al.* 1994), implemented at 1/16th degree resolution, as the primary tool in assessing hydrologic changes over the Pacific Northwest (Chapter 5, this report; Elsner *et al*. 2010). Fine-scale hydrologic models, however, have the potential to improve these simulations via higher spatial resolution, a more explicit representation of fine-scale watershed processes, and additional simulation variables (such as water temperature). These advantages would probably be most apparent in relatively small watersheds and would support a primary objective of the CBCCSP to increase coverage of small-scale watersheds in the PNW to facilitate water resource planning. Despite potential advantages, fine-scale hydrologic simulation models are very expensive to implement, and also require more computer resources both to run the models (CPU time) and to archive the model output (disk space). Do these more explicit fine-scale simulation models provide the added value that would justify their increased implementation, run time and storage costs? In this chapter we explore this question in detail by comparing and contrasting the climate change scenarios produced using a macro-scale hydrologic model (VIC) and the Distributed Hydrologic Soil Vegetation Model (DHSVM), a fine scale hydrologic model, implemented over a set of medium-sized test watersheds in Washington State (WA) (see Section 1.3).

2. Overview of Hydrologic Models Used in the Inter-comparison Study

Figures 1 and 2 show schematic diagrams of DHSVM and VIC, respectively. As noted above, the VIC land surface hydrology model, forced by gridded observed and future meteorological variables, is the primary tool used in the CBCCSP for creating hydrologic scenarios. This model has most recently been implemented at 1/16th degree latitude-longitude resolution (Chapter 5 of this report; Elsner *et al*. 2010). The VIC model uses a water balance time step of 24 hours, but simulates snow processes at sub-

daily time steps of 1 hour. The model also incorporates up to five sub-grid scale elevation bands, each associated with a mosaic of vegetation types. VIC solves the surface water budget for each of these elevation bands and vegetation types, and then aggregates the final results using a simple area weighted average (Liang *et al*. 1994). VIC employs a sophisticated, energy balance snow model that accounts for important canopy processes in forested watersheds (Andreadis *et al*. 2009).

We compare the results from VIC to those generated by DHSVM (Wigmosta *et al.* 1994), which explicitly represents the effects of topography and vegetation on water fluxes through the landscape. DHSVM was developed to simulate hydrologic processes in mountain watersheds with relatively steep slopes, and has been widely applied and validated in the Pacific Northwest region. DHSVM is typically implemented at high spatial resolutions on the order of 100 m^2 for watersheds with and area of about 10,000 km^2, although many implementations are for watersheds with basin areas of less than 1000 km^2. Sub-daily time steps ranging from about 1 to 3 hours are used for multi-year simulations, depending on the spatial scale. DHSVM applies essentially the same energy balance snow model as VIC, however the forcings for the model are quite different on a grid cell basis, since DHSVM explicitly accounts for slope and aspect to characterize shortwave and longwave radiation affecting the surface energy balance.

Both VIC and DHSVM, as with any fully distributed hydrologic models, require extensive information about the simulated basin. The first type of information is static data and can be divided into three main categories: elevation, vegetation cover and soil type. The second type is dynamic, or timeseries, information, including meteorological driving data obtained from weather stations or derived from other models. For the 5 sub basins modeled in this inter-comparison (see Section 1.3), observing stations do not have sufficiently long records or do not exist in a spatially relevant location. Therefore, gridded meteorological products are used to provide the spatial coverage needed for each model (Chapter 3, this report).

In contrast with VIC, which parameterizes fine-scale topographic features using elevation bands, the fine-scale topography in DHSVM is explicitly represented via Digital Elevation Model (DEM) elevation nodes. DEM data are used to define absorbed shortwave radiation, precipitation, air temperature, and down-slope water movement. Another important difference between DHSVM and VIC is that in a VIC implementation each cell is assumed to be big enough to remain isolated from others (i.e. water transfer from the soil boundary between cells is much smaller than streamflow) whereas in the DHSVM each cell exchanges surface and subsurface water with its neighbors resulting in a three-dimensional redistribution of water across the basin. This water is routed across the basin using the defined stream channel network. In the VIC implementation a post-processing routing scheme in used simulate streamflow based on a flow direction file and daily runoff and baseflow estimates from each grid cell.

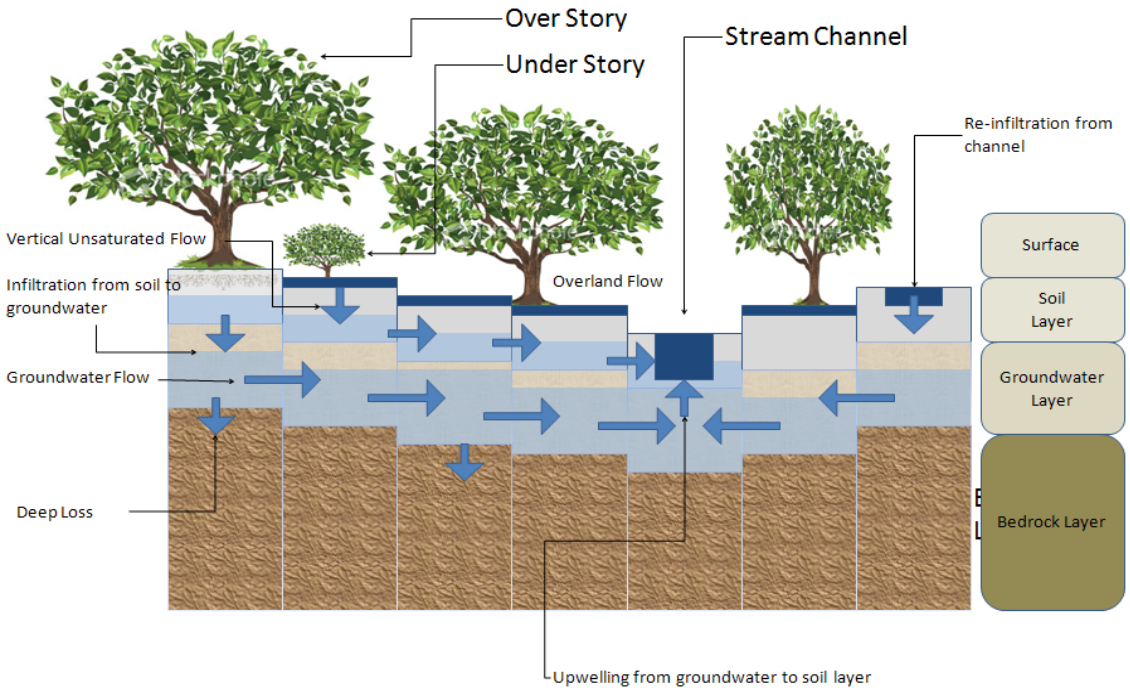

Figure 1 DHSVM conceptual model

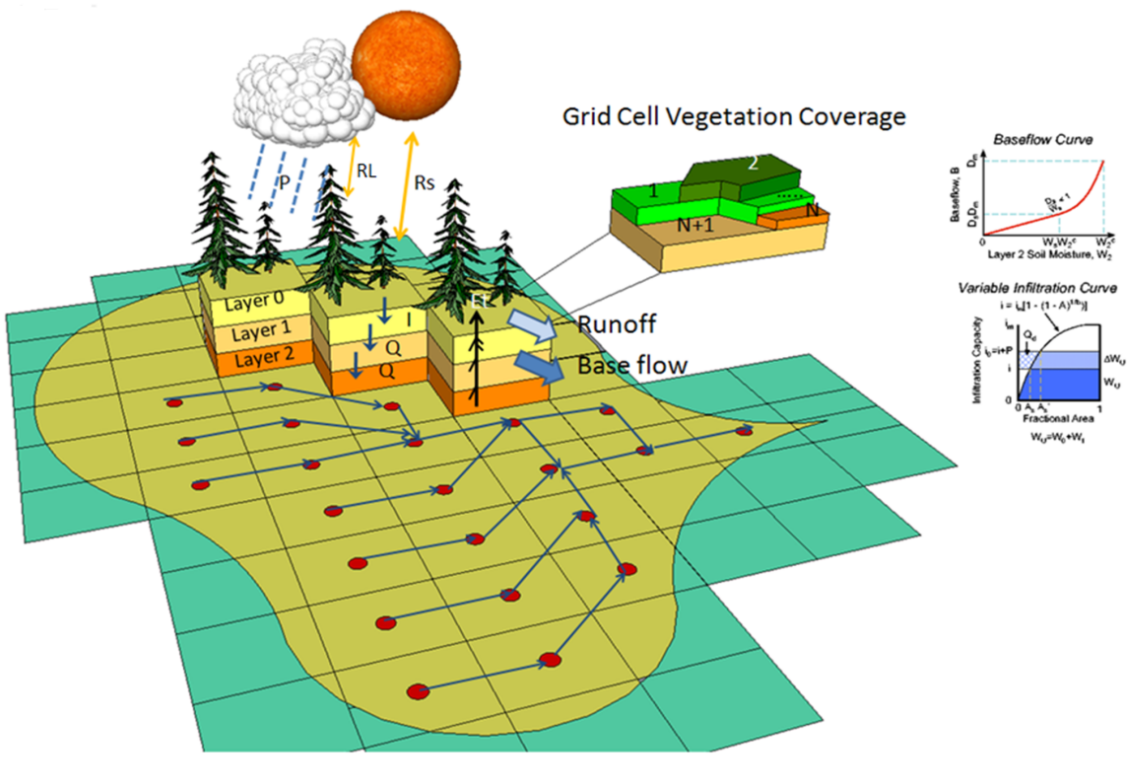

Figure 2 VIC conceptual model

3. Approach/Methods

3.1 Case Study Watersheds

The DHSVM was applied to the following sub basins of the Columbia River: Upper Yakima, Naches, Methow, West Kettle and Walla Walla. For each sub basin, Table 1 summarizes the main characteristics of the watershed, Table 2 contains the predominant vegetation types and Table 3 includes the soil types.

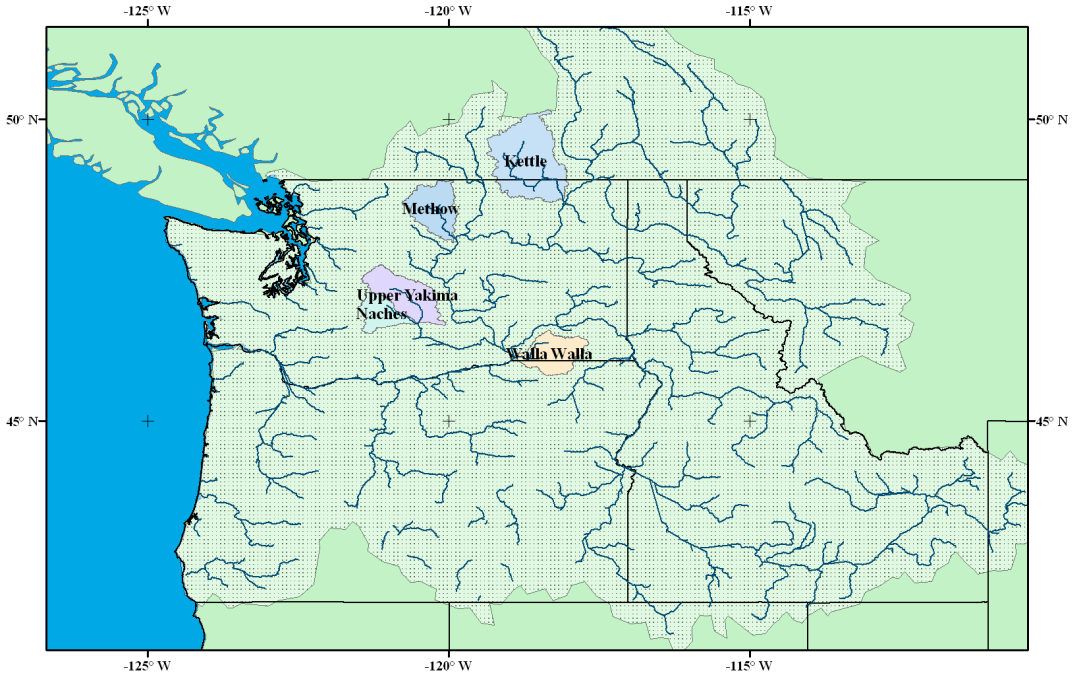

Figure 3 Location of the sub basins analyzed.

3.1.1 Upper Yakima

The Upper Yakima River is a tributary of the Yakima River in central Washington State. The river rises in the Cascade Range at Keechelus Dam on Keechelus Lake near Snoqualmie Pass, northwest of Cle Elum.

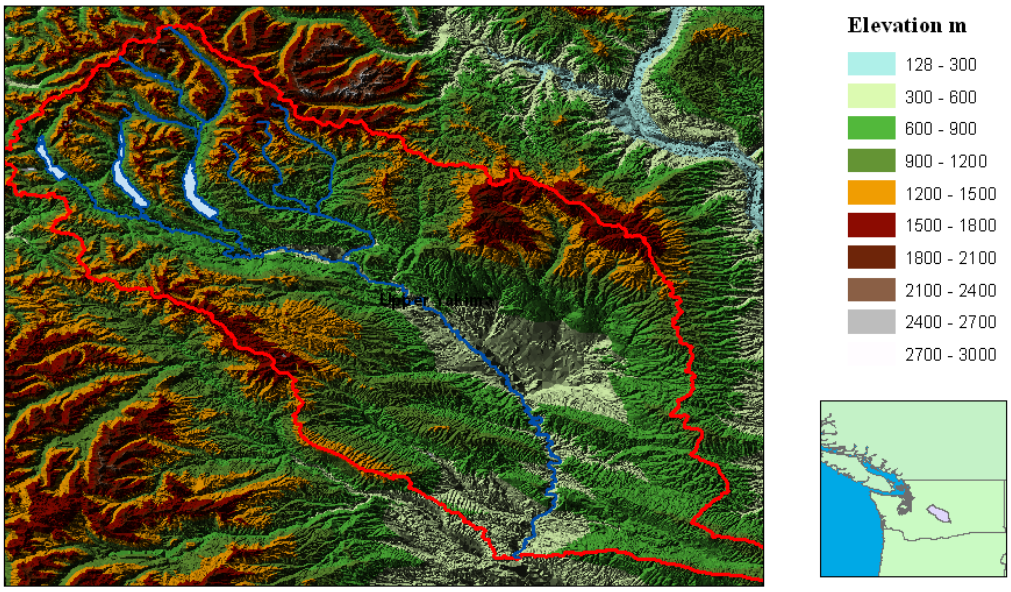

Figure 4 Map of the Upper Yakima basin.

3.1.2 Naches

The Naches River is also a tributary of the Yakima River in central Washington. Beginning as the Little Naches River, it is about 75 miles long. After the confluence of the Little Naches and Bumping River, the river's name becomes simply the Naches River. The Naches and its tributaries drain a portion of the eastern side of the Cascade Range, east of Mount Rainier and northeast of Mount Adams. In its upper reaches, the Naches River basin includes rugged mountains and wilderness. The lower Naches River and its tributary, the Tieton River, flow through valleys with towns and irrigated orchards northwest of Yakima, where the Naches River joins the Yakima River.

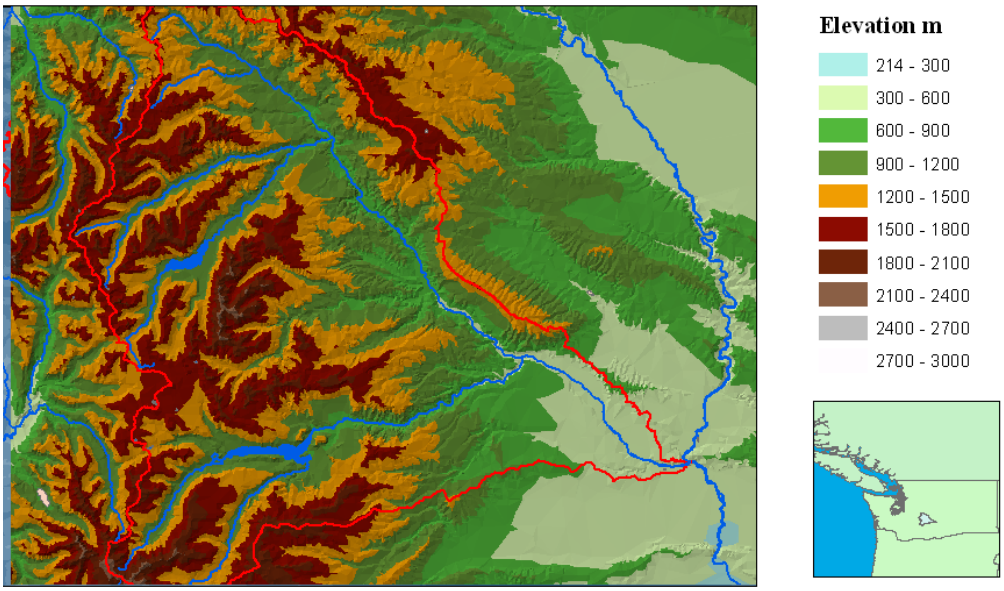

Figure 5 Map of the Naches basin.

3.1.3 Walla Walla

The Walla Walla River is a tributary of the Columbia River, joining the mainstem Columbia just above Wallula Gap in southeastern Washington State. The river flows through Umatilla County, Oregon and Walla Walla County, Washington. The headwaters of the Walla Walla River lie in the Blue Mountains of northeastern Oregon. The river originates as the North and South Forks of the Walla Walla River.

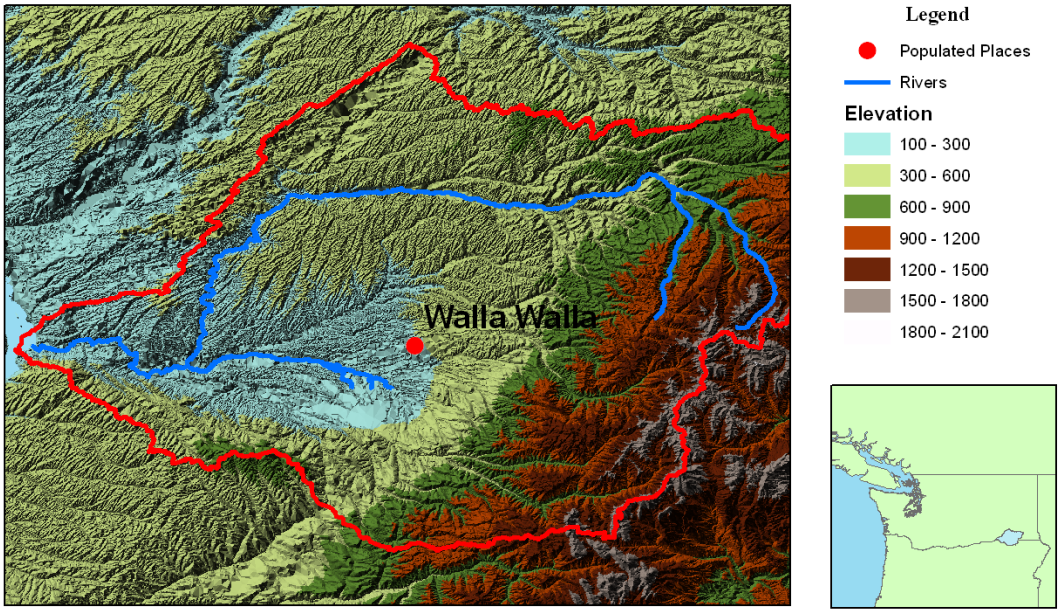

Figure 6 Map of the Walla Walla basin

3.1.4 Methow

The Methow River is a tributary of the Columbia River in northern Washington State. The Methow River, along with its tributaries, Twisp River, Cedar Creek, and Early Winters Creek, originate in a cluster of the high mountains, including the Golden Horn, Tower Mountain, Cutthroat Peak, Snagtooth Ridge, Kangaroo Ridge, Early Winter Spires, and Liberty Bell.

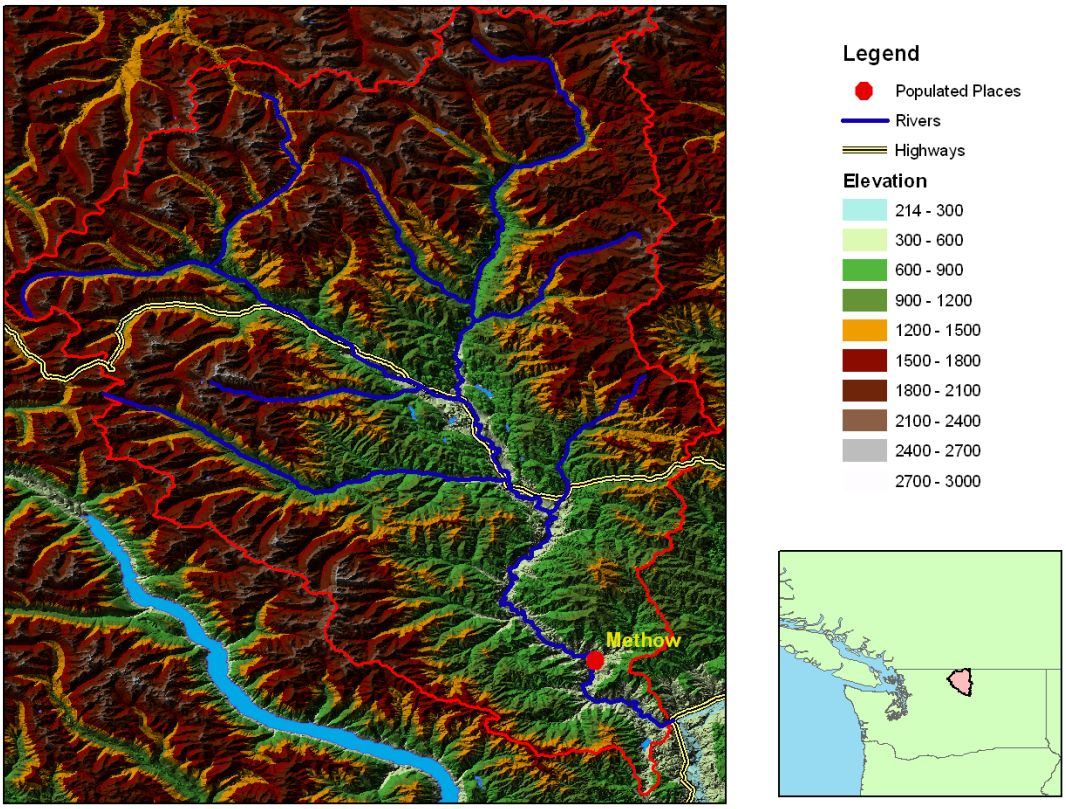

Figure 7 Map of the Methow basin

3.1.5 West Kettle

The West Kettle River is a tributary of the Kettle River in southern British Columbia. The Kettle River is a tributary of the Columbia River, joining it near Kettle Falls, Washington. The Columbia River at this point is a large reservoir called Lake Roosevelt.

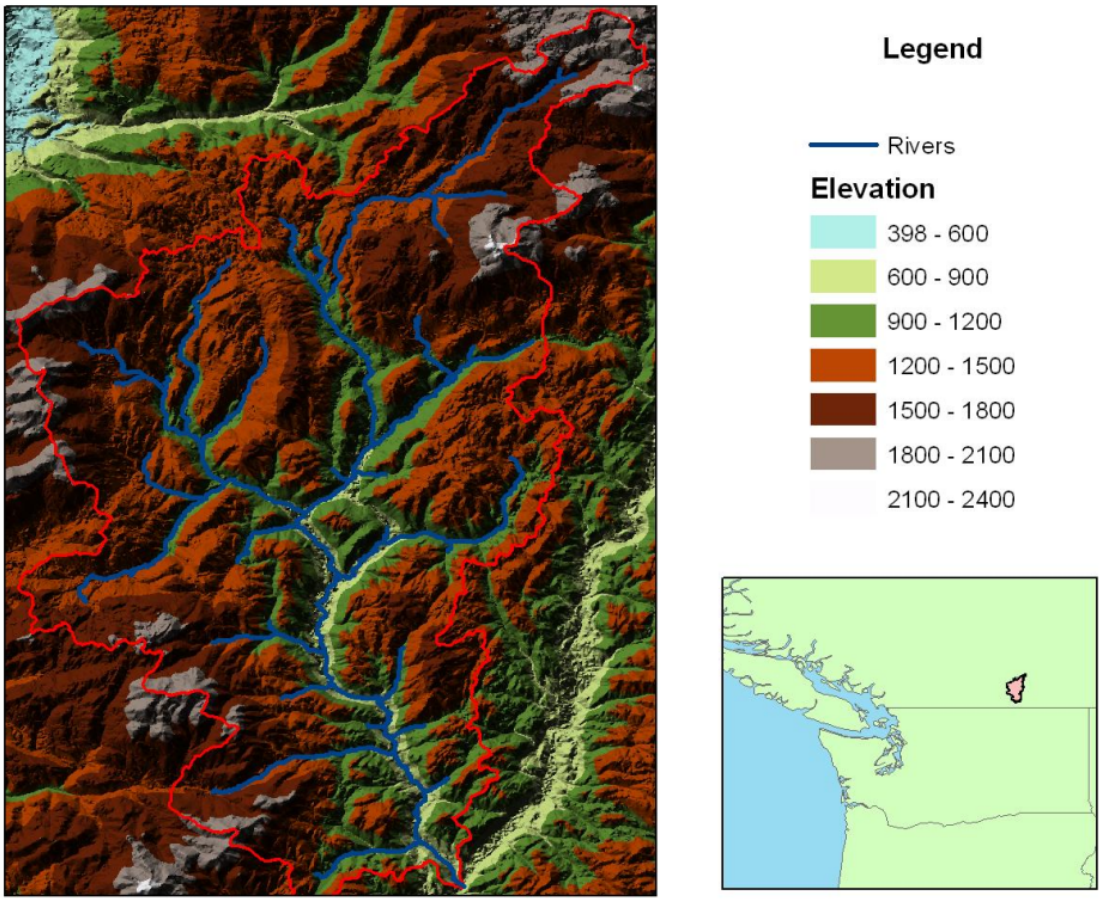

Figure 8 Map of the West Kettle basin

Table 1 Main characteristics of each study watershed.

	Upper Yakima Basin	Naches Basin	Walla Walla Basin		Methow Basin	Upper Kettle Basin
			Blue Mtns	Lowlands		
Drainage Area (sq. km.)	4144	2875	4293		4620	1870
Maximum Elevation (m)	2388	2496	1905	270	2674	2307
Minimum Elevation (m)	414	329		80	284	626

Table 2 Vegetation types found within each study watershed.

Vegetation Type	Upper Yakima Basin	Naches Basin	Walla Walla Basin	Methow Basin	Upper Kettle Basin
Evergreen Needleleaf	52%	72%	19%	60%	50%
Deciduous Needleaf	0%	0%	0%	0%	30%
Open Shrub	27%	17%	12%	23%	0%
Grassland	11%	4%	1%	11%	0%
Cropland	6%	4%	56%	0%	0%
Urban	0%	0%	4%	0%	1%
Closed Shrub	0%	0%	6%	0%	18%
Bare land	0%	0%	0%	4%	1%

Table 3 Soil types characterizing each study watershed. Empty boxes indicate that these soil types are absent from the basin.

Soil Type	Upper Yakima Basin	Naches Basin	Walla Walla Basin	Methow Basin	Upper Kettle Basin
Sandy Loam	36%	19%	23%	25%	29%
Loam	37%	50%	5%	27%	0%
Silty Loam	16%	19%	54%	47%	31%
Bedrock	5%				0.001%
Sandy			23%		39%
Sand			2%		0%

3.2 VIC Implementation

Chapter 5 of this report provides a complete description of the VIC model implementation used in the CBCCSP project and its calibration (see also Elsner *et al.* 2010). The calibrated results of this implementation were generally used in this inter-comparison study. However, in order to boost the accuracy of VIC in these small-to-medium sized basins, the analyses incorporated fractional coverage of edge cells. In this process the simulated runoff and base flow from each cell was prorated based on the percentage of the cell overlapping with the basin. This approach avoids overestimation of the contributing basin area.

Figure 9 shows an example for the Upper Yakima Basin. Cells located at the edge only have a fraction of their area within the basin, therefore only the equivalent percentage of base and stream flow was included in the routing scheme.

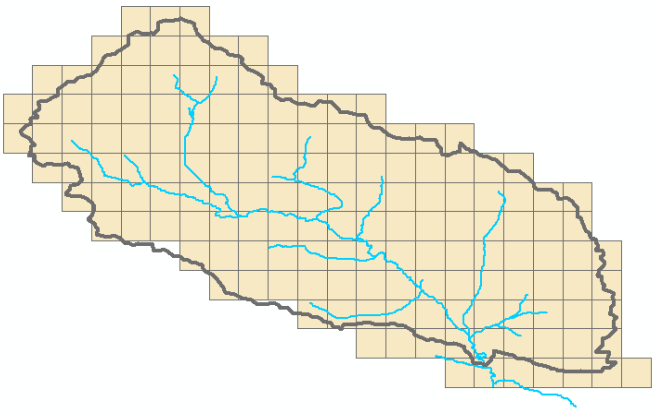

Figure 9 VIC cells over the Upper Yakima River Basin

Additionally, the West Kettle Basin VIC implementation was calibrated manually, because the original project calibration did not satisfactorily simulate the observed streamflow values.

3.3 Distributed Hydrology Soil Vegetation Model Implementation

In this study, we implemented the version of DHSVM v2.4. Improvements to the previous versions were incorporated to include the following features: a deep groundwater layer, the expansion of surface and subsurface flow paths from 4 to 8 directions, the allowance for a re-infiltration of water from the stream channel network back into the adjacent soil layer, the division of surface flows generated by runoff from impervious surfaces as a fraction of impervious area, and the calculation of water temperature within the channel network.

DHSVM (Wigmosta *et al*. 1994; Wigmosta *et al.* 2002) is a spatially explicit hydrologic model that accounts for the physical processes affecting the movement of water on and through the land surface with a distributed, deterministic approach. In general, the model dynamically represents the spatial distribution of evapotranspiration, snow cover, soil moisture, and routed runoff across a watershed (Wigmosta *et al*. 2002). The DEM serves as the spatial basis for the model's physical processes and DHSVM can solve full water and energy balance equations at the resolution of a DEM. The typical spatial resolutions for model applications range from 30-200 m (VanShaar *et al*. 2002). The DEM resolution drives the topographic controls on model processes including: absorbed solar radiation, net longwave radiation, precipitation, air temperature, and downslope water movement (Wigmosta *et al*. 1994).

The model relies on a two-layer vegetation representation and a multi-layer soil profile for each pixel within the watershed boundary. For each pixel, any combination or number of individual soil and vegetation classes may be incorporated, thereby enhancing the ability of the model to represent basin characteristics. We use three soil layers and a single vegetation class for each pixel in this case. The model operates at the same time step as the meteorological inputs, allowing as fine as 1-hr temporal resolution. For the studies described here, a three-hourly time step is used.

DHSVM incorporates a sophisticated two-layer snow accumulation and ablation model, which relies on an energy balance that includes the effects of local topography and vegetation cover (Wigmosta *et al*.1994; Andreadis *et al*. 2009). Surface and

subsurface flow routing algorithms channel water to the watershed outlet and allow grid cells to exchange water with adjacent neighbors (Wigmosta *et al.* 2002). The inputs to DHSVM can be divided into three separate groups: 1) spatial data including raster and vector inputs, 2) meteorological time series data, and 3) associated files that serve as look-up tables during the modeling.

Spatial data inputs include a DEM, a watershed mask, and grids of the soil type, soil depth and vegetation type. The stream and road networks are included as vector data. The model forcings are a time-series of meteorological variables, primarily precipitation, temperature, shortwave and longwave radiation, relative humidity and wind. The various text file look-up tables provide physical details about the types of meteorological, soil, and vegetation data used. DHSVM utilizes a cell-by-cell approach to move water through the hydrologic system. A more detailed description of the individual modules within the main DHSVM follows.

3.3.1 Evapotranspiration

DHSVM estimates evapotranspiration (ET) based on a potential ET (PET) rate calculated using the Penman-Monteith approach. The model represents the canopy or overstory and understory with a two-layer vegetation input. The model enables the overstory to remove water from both the upper and lower soil zones, while the understory can only remove water from the upper zones. Solar radiation and wind speed are attenuated through the two canopies based on cover density and leaf area index (LAI). Soil water evaporation is dependent on PET demand (as above), modulated by the soil's ability to supply water in the rooting zone (Wigmosta et al., 1994). When snowpack is present in the simulations, it is assumed to cover the complete grid cell; consequently, no evapotranspiration from the soil or understory layer is calculated when snow cover is present in any grid cell. DHSVM also accounts for a wet and dry fraction in the vegetative layers, which enables the model to account explicitly for interception, storage, and through fall.

Separate shortwave and longwave radiation budgets are developed for both for the vegetation overstory and understory. The overstory receives direct solar radiation (shortwave) and the reflected longwave radiation with both the sky and the understory or soil. The understory also receives attenuated shortwave radiation and exposed understory receives direct shortwave radiation. Finally there is also exchange of longwave radiation between the understory and the ground. Shortwave incoming radiation (beam and diffuse) and diffuse longwave radiation from the sky are supplied to the model (Wigmosta, 2002).

3.3.2 Two-Layer Ground Snowpack Model.

DHSVM simulates the processes of accumulation and melt of the snowpack using the two–layer, energy- and mass-balance described by Storck and Lettenmaier (1999) and Andreadis *et al.* (2009). The model also estimates energy exchanges occurring between the atmosphere, overstory canopy, and main snowpack. The energy balance components of the model solve snowmelt, refreezing, and changes in snowpack heat content, whereas the mass-balance equations solve the snow accumulation and ablation processes, transformations in the snow water equivalent, and snowpack water yield (Wigmosta, 2002). The model also estimates the changing snow surface albedo, based on the number of days since the last new snow (Laramie and Schaake, 1972).

3.3.3 Canopy Snow Interception and Release

DHSVM represents canopy snow processes utilizing a one-layer mass and energy balance model (Storck and Lettenmaier, 1999; Storck, 2000; Andreadis *et al.* 2009). This component of the model explicitly represents the topographic and vegetative influences on the energy and mass exchanges that occur on the snow surface, particularly the processes governing snow interception, sublimation, mass release, and melt from a forest canopy. Atmospheric precipitation is classified as rain and snow based on atmospheric temperature thresholds on the grid cell and time step, where the user defines minimum and maximum temperatures for rain and snow occurrence. The volume of intercepted snow is determined by the efficiency of the process, which is dependant of the leaf area ratio and temperature. This formulation is based on field observations by Storck (2000).

3.3.4 Unsaturated Soil Moisture Movement

Unsaturated moisture movement is simulated using a multi-layer representation based on the two-layer model described by Wigmosta *et al.* (1994). Each soil surface cell may remove water by way of the mechanisms of throughfall, snowmelt, or surface runoff from adjacent cells. The user defines the maximum infiltration rate, which is used by the model to calculate infiltration into the upper soil layer. Excess water above infiltration capacity estimates enters the surface routing components of the model. When water has infiltrated into the unsaturated soil profile, it is able to percolate through the additional layers. This process is controlled using Darcy's Law and the Brooks-Corey relationship (Brooks and Corey, 1964).

Infiltrated water may be removed from the unsaturated profile through the following processes: ET from the upper soil layer; transpiration is also possible from inside the soil profile depending on the total percent of plant roots in a soil layer; and lastly, desorption from the top soil layer may occur and is calculated based on the work of Eagleson (1978).

3.3.5 Saturated Subsurface Flow

DHSVM employs both a kinematic and a diffusion approach to route saturated subsurface flow downslope cell by cell. The kinematic method uses slopes to approximate the hydraulic gradient for those cells representing steep areas with thin, permeable soils. However, for areas of low vertical relief, the diffusion assumption is utilized to approximate hydraulic gradients using local water table slopes (Wigmosta *et al.* 2002).

Subsurface water moving downslope to a channel may be intercepted by a road segment. Road segment interception occurs when a road cut depth exceeds the depth to the water table. Channel interception occurs similarly.

3.3.6 Overland Flow

Generation of runoff flow occurs when at least one of three physical conditions is met. First, overland flow occurs when the sum of throughfall and snowmelt exceeds the user-defined infiltration capacity. Second, runoff may also be generated if throughfall or snowmelt occurs on a cell with fully saturated soil layer. Finally, runoff is also possible if the water table rises above the soil surface. (Wigmosta *et al*. 2002).

Runoff is routed on a cell-by-cell basis downslope in a similar way to subsurface routing. Basically, the overland flow algorithms account for cell size, the volume of the surface water, and the amount of water leaving the system via culvert outflow. The model uses a constant water velocity (Wigmosta *et al.* 2002).

3.3.7 Channel Flow

Water enters the channel network via subsurface contributions of lateral inflow, direct delivery from overland flow or culvert outflow from a road channel. Flow through the network of road ditches and stream channels is routed using a cascade of linear channel reservoirs. Each channel segment represented in the model has uniform hydraulic properties. The user is able to assign hydraulic properties to individual road or stream classes, including length, width, depth, roughness, and channel slope during the preprocessing of the road and stream. These constants assign a constant flow velocity per channel segment and time step that is calculated from Manning's equation (Wigmosta *et al*. 2002).

3.3.8 Water Temperature

The stream temperature component of DHSVM calculates a radiative energy balance in each channel segment at each time step (Figure 10). Additionally, the model accounts for the flux of heat associated with the flow of water into and out of each segment. The model is based on the radiative heat balance model described by Chapra (1997). The model makes use of the existing gridded metrological forcing information

and requires only a few calibration parameters in the configuration file and an additional stream class property (the mixing ratio) in the stream-class.dat file.

$$\frac{dT_s}{dt} = \frac{Q}{V}T_{in} + \frac{J_{DS}}{\rho C_p H} + \frac{J_{AL}}{\rho C_p H} - \frac{Q}{V}T_{Out} - \frac{J_{WL}}{\rho C_p H} - \frac{J_{COND}}{\rho C_p H} - \frac{J_{EVAP}}{\rho C_p H}$$

Jds: Heat from direct solar radiation

Jal: Heat for atmospheric longwave radiation

Jwl: Longwave re-emitted from water surface

Jcond: Conduction heat exchange with atmosphere

Jevap = Heat excange from evaporation (function of windspeed)

QT/V: Heat conveyed by mass flow into and out of segment.

From: Chapra, S.C., Surface Water Quality Modeling. 1997, McGraw-Hill.

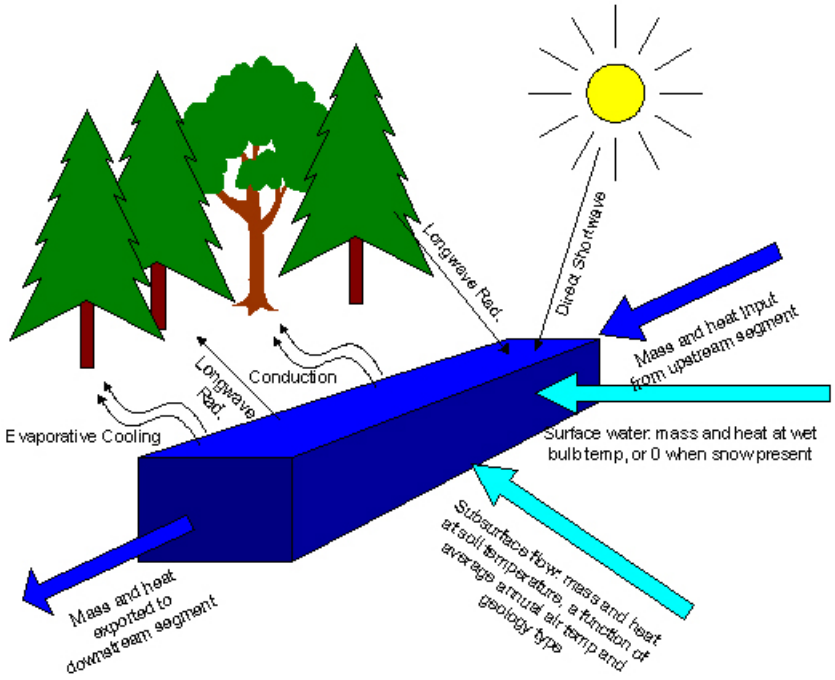

Figure 10 Stream Temperature Heat Balance Equation

3.4 Preprocessing

There is a basic progression of preprocessing steps completed for each of the basins. Implementation of the DHSVM in these basins basically involves GIS preprocessing of the necessary spatial inputs, collection and formatting of meteorological drivers, formatting the necessary configuration files. Figure 1111 summarizes the sequence of preprocessing steps.

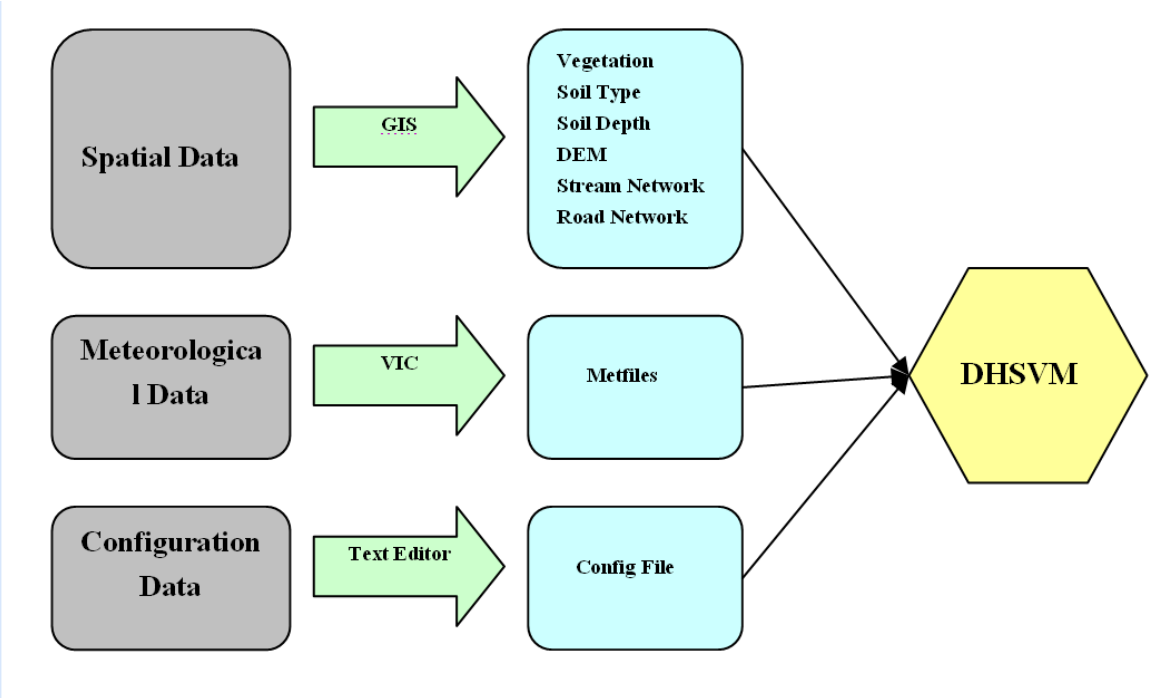

Figure 11 Preprocessing schematic diagram. This figure illustrates the three preprocessing steps needed to implement the model for a location.

3.4.1 GIS Preprocessing

While DHSVM is not directly linked to any particular Geographical Information System (GIS), the inputs and outputs are best managed within ArcGIS from ESRI. Spatial data was obtained from diverse sources and compiled, edited, and formatted using ArcGIS 9.2. The basic inputs to the model are elevation, soil types, vegetation types, road network and stream network. From this spatial information it is possible to generate the following inputs: soil depth, terrain shadowing and percent of open sky.

3.4.1.1 Raster Data

Seamless 30-m and 90-m resolution digital elevation models were obtained for each watershed from the National Elevation Dataset (United States Geological Survey, National Map Seamless Server, 2009). Since the model is unable to handle sinks in the topography the input Digital Elevation Model (DEM) was reconditioned in ArcInfo in order to produce a smooth model for hydrologic simulations. This reconditioning is an ArcHydro process that ensures a linear drainage pattern onto the model grid. This is done

through two basic methods: 1) filling in sinks in the drainage area by raising the elevations of those grid cells, and 2) lowering the elevation of the cells corresponding with the vector drainage network, efficiently burning the channel network into the DEM. Refer to Figure 1212 for an example DEM input file.

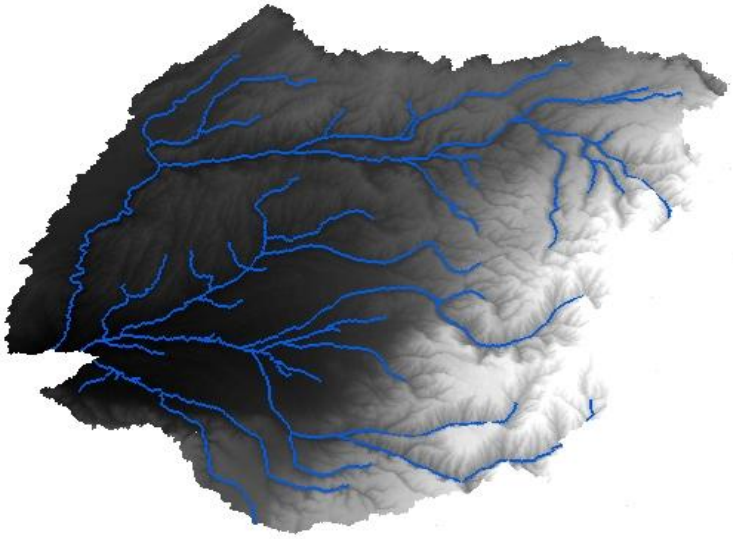

Figure 12 Example of a watershed DEM input file.

Soils spatial data were obtained online from the United States Department of Agriculture Natural Resources Conservation Service (USDA NRCS). The datasets used is the Soil Survey Geographic Database (SSURGO; Soil Survey Staff, 2006). The SSURGO data provide soil information at a scale of 1:24,000 (Figure 13).

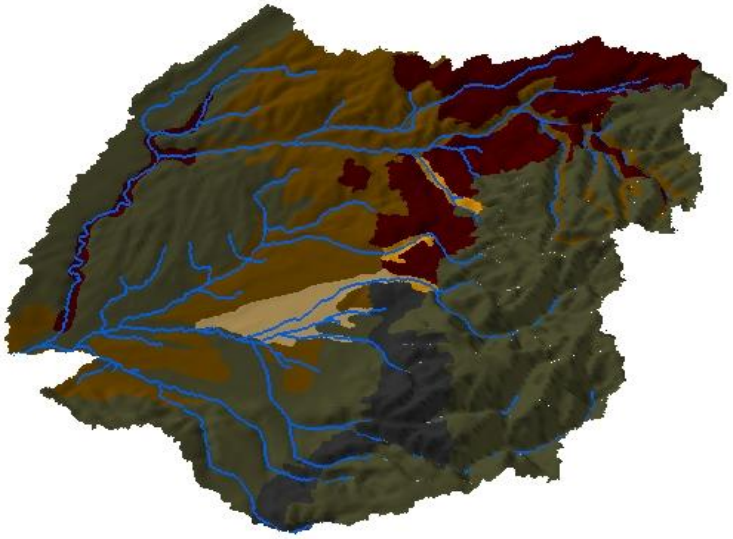

Figure 13 Example of a watershed soil input file.

A soil depth grid is also needed for model input (Figure 14). The depth of the soil profile corresponding to specific soil types is generally known information; however, this is not an available spatial data layer. DHSVM incorporate an ARCinfo script that generates a soil depth grid in ArcInfo for input into the model. This raster is created as a function of the watershed slope and a range of soil profile depths based on the soil type.

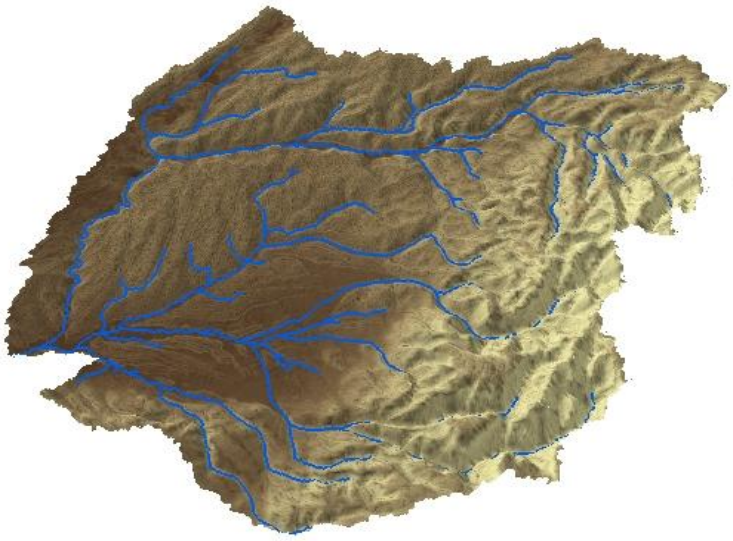

Figure 14 Example of a watershed soil depth input file.

Vegetation cover data at 30-m resolution were obtained online from National Land cover Database (NLD) datasets (2001). These data were derived using Landsat TM-7 imagery to classify the vegetative cover. The level of detail provided by NLD is not necessarily appropriate for DHSVM input, particularly because the data to accurately describe the differences in the physical parameters of some vegetation types is not available. Due to this fact, the vegetation grid was reclassified into fewer classes utilizing ArcMap (Figure 15).

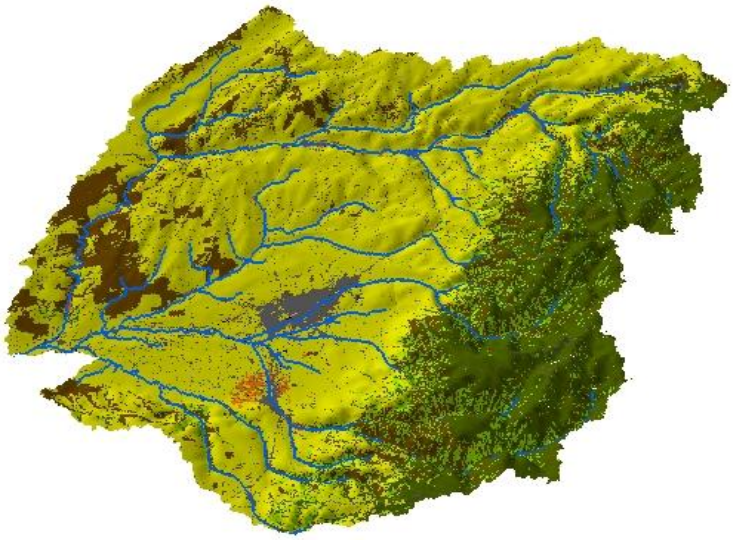

Figure 15 Example of a watershed vegetation input file.

The model ensures that every pixel from the input data is associated with a grid cell in the watershed. The DHSVM uses a mask of the watershed area to select only those cells within the watershed boundary for analysis. This process ensures that the limits of the area of interest are the same for every spatial elevation, soil type, soil depth, and vegetation type file. This mask raster is created using the ArcHydro 1.3 Batch Watershed Delineation Tool. By working through a series of terrain preprocessing steps, each pixel in a DEM is assigned a flow direction. ArcHydro can then delineate a watershed polygon from any point specified within the raster by selecting all pixels that collectively drain to that point. Subsequently, the 'Feature to Raster Tool' in ArcToolbox converts this polygon feature class to a 30-m resolution grid. Ultimately, this mask raster of the watershed is used in the model to extract the drainage basin values from the soil type, soil depth, vegetation type, and DEM raster inputs (Figure 16).

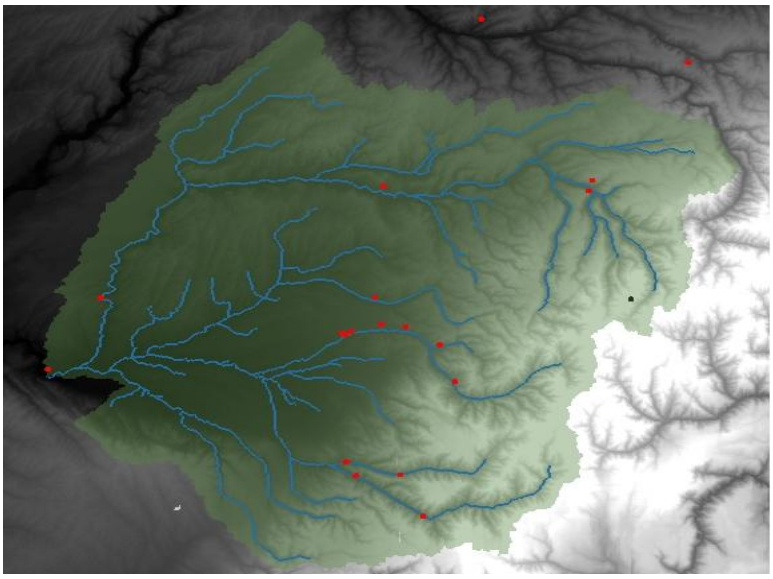

Figure 16 Example of a watershed mask input file.

3.4.1.2 Vector Data

DHSVM requires roads and stream networks within the watershed extent. Digital spatial data of the road network is located at University of Washington's Washington State Geospatial Data Archive (WAGDA). Stream network data were obtained through the Washington State Department of Ecology Geographic Information System web site. However, these hydrologic data are only used as a digital layer for mapping purposes, locations and identity of named stream reaches. These data are not used as the stream coverage for input into DHSVM since the generation of a continuous stream network with assigned flow direction per segment is a required preprocessing step in the model.

The STREAMNETWORK Arcinfo script creates a stream network with streamflow topology based on the reconditioned DEM, the watershed of interest previously delimited, and a stream initiation threshold defined by an area in meters sq., m^2 (Figure 17).

The contributing watershed area parameter for stream initiation recommended by Storck *et al.* (1998) is a minimum surface of 20,000 m^2 for small catchments on the west

slopes of the Cascades Range in Washington State. On the drier east side of the Cascades Doten and Lettenmaier (2004) used a stream initiation area of 40,000 m^2.

The road system definitions file is created in a similar way using the ROADNETWORK script in ArcInfo.

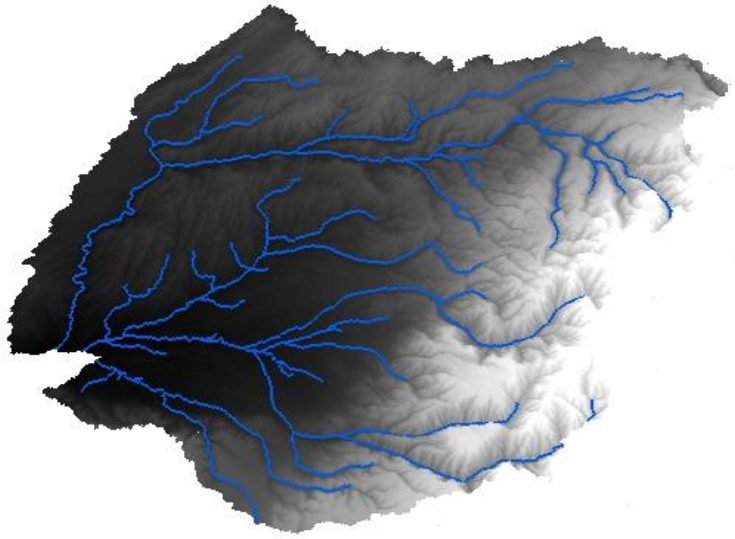

Figure 17 Example of a watershed stream network map.

3.4.2 Meteorological Data

DHSVM implementations typically use meteorological records associated with a group of nearby weather stations. The model distributes weather parameters within the watershed modeled, for each time step, using an interpolation scheme. The model requires the following meteorological data files for each time step and weather station defined: air temperature (°C), wind speed (m/s), relative humidity (%), incoming shortwave radiation (W/m^2), incoming longwave radiation (W/m^2), and precipitation (m/time step). However, the existing network of meteorological observing stations in the U.S. does not cover the degree of spatial and temporal coverage necessary to drive this micro scale model in some of the basins of interest. Under these conditions, it is often necessary to use a gridded product that is derived statistically from the observing network of meteorological stations. The gridded product has already gone through a series of quality control processing steps, which facilitates getting it 'model ready'. Also, these products are more conducive to the downscaling approaches used to derive local data

from the global circulation model (GCM) scenarios used in conducting climate change experiments.

A 1/16th gridded data set developed by the University of Washington that covers the PNW and Canada was used to provide gridded input (Figure 18). Chapter 3 (this report) describes how this data set was derived using the methods of Hamlet and Lettenmaier (2005). This data set contains precipitation, air temperature (maximum and minimum) and wind speed at daily intervals. Since these parameters are not sufficient to run DHSVM, the meteorological pre-processor in the VIC model was used to generate the additional forcings for each cell: relative humidity (%), incoming shortwave radiation (W/m^2), incoming longwave radiation (W/m^2), and precipitation (mm/time step). This process also enables the reduction of the time scale from daily to the 3 hourly time steps required by the DHSVM. The VIC output files for wind speed still need to be processed at the same height required by DHSVM. In order to produce these data a procedure defined by Arya (1998) to scale the wind was applied.

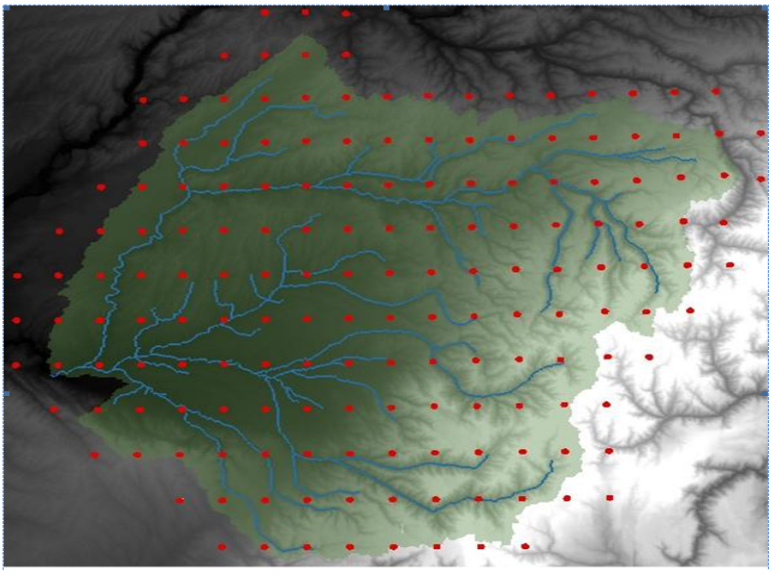

Figure 18 Example of a watershed gridded meteorological station input file.

For each of the test watersheds, 10 different climate change scenarios were run based on the hybrid delta downscaling method discussed in Chapter 4 of this report.

3.4.3 Configuration File.

The DHSVM requires an ASCII configuration file that serves as a reference table for the values describing the physical conditions of the basin. The configuration file allows the model to interpret the thematic spatial inputs, and therefore, is generally where modifications are made to change the outputs. DHSVM is capable of simulating any number of soil or vegetation types in a watershed. Each of the vegetation types may consist of two individual vegetative layers, and each soil types may be composed of many soil layers. The inventory of physical values necessary to describe each individual soil and vegetation layer is extensive. Furthermore, many of the parameters used in model calculations are obscure and are not readily available in the literature for each unique soil and vegetation type. Thorough completion of the configuration file using cited values for soil and vegetation parameters is time-intensive, so some generalization is necessary. However, the aim in this case was to parameterize the model for the calibration run using the best available referenced values.

3.5 Model Calibration

Calibration techniques for the DHSVM are dependent on the information available during the implementation. Whitaker et al (2003) defined a three-step approach to calibrate a basin. The first step adjusts parameters dealing with snow melt and accumulation in non-forested areas; then parameters affecting melt and accumulation below the canopy; and finally, the soil parameters affecting runoff generation. The calibration of soil parameters is discussed by Storck *et al.* (1998) uses parameters, such as depth of the rooting soil layers, depth of soil below the rooting zones and lateral saturated hydraulic conductivity, to calibrate to observed basin outflow hydrographs.

A normal approach in the DHSVM is to adjust precipitation by a factor proportional to the discharge of the basin. This process consists of multiplying or scaling precipitation within the basin to obtain a fixed factor between it and the annual discharge. Those factors are empirical numbers based on observations within the basin under the same conditions. Wigmosta *et al*. (1994) indicated that the model was calibrated to

annual discharge by multiplying the elevation-corrected precipitation by an additional 16%. A similar strategy was also employed by Stock *et al.* (1998) in the PNW, by Palmer and Hahn (2002) in Oregon, and by Whitaker *et al*. (2003) in a small catchment in B.C. Similar correction factors as high 20% have been used in other studies (Linsley *et al.* 1982; Legates and DeLiberty 1993; Palmer and Hahn 2002).

Although commonly used, the above approach was not used to calibrate DHSVM in these implementations, in order to maintain consistency between the meteorological inputs of VIC and the DHSVM. Since the models were implemented using all the gridded meteorological files available for the basins, it is not possible to use temperature lapse rates as a calibration tool. Therefore only soil, geological, and vegetation parameters were adjusted to obtain the proper monthly and annual discharge. As noted above, deep ground water simulation was also not implemented in DHSVM in order to maintain rough parity with the physical processes incorporated in VIC.

Calibration of VIC was carried out using an approach similar to Matheussen *et al.* (2000) and is reported in more detail by Elsner *et al.* (2010) and Chapter 5 (this report). In this approach major sub-watersheds were identified and the routed streamflow was calibrated at a monthly time step.

Table 4 Summary error statistics for DHSVM calibration for 5 case study watersheds.

Calibration period (1985-1988) Validation period (1988-1989)									
Basins (gage)	Annual mean					N-S model efficiency			
	Obs. (cfs)	Sim VIC (cfs)	Sim. DHSVM (cfs)	Sim/Nat VIC (%)	Sim/Nat DHSVM (%)	Calib. VIC (monthly)	Calib. DHSVM (monthly)	Valid. VIC (monthly)	Valid. DHSVM (monthly)
Naches River at Naches	1337 **	1615	1733	1.23	1.32	0.62	0.64	0.64	0.41
Kettle River at Westbridge	1337 *	568	628	1.63	1.80	0.40	0.12	0.41	0.34

WallaWalla River at Touchet	425 *	1326	1334	3.12	3.14	-0.12	0.16	-0.12	0.11
Methow River at Pateros	1174 *	1586	1134	1.43	1.02	0.80	0.83	0.72	0.80
Upper Yakima at Cle Elum	1677 **	1735	1752	1.03	1.03	0.86	0.73	0.88	0.80

* Observed flow (naturalized data was unavailable)

** Estimated natural flow

4. Model Results

4.1 Kettle

Table 5 Change in streamflow for the climate change simulation expressed as a percent change with respect to the historical runs.

Kettle						
Scenario	Cold Season % Change		Warmth Season % Change		Year % Change	
	VIC	DHSVM	VIC	DHSVM	VIC	DHSVM
ccsm3	63.5	41.6	-23.5	-16.4	1.8	0.2
echam5	65.9	49.7	-17.9	-14.6	6.5	3.8
hadgem1	51.0	30.8	-35.8	-27.7	-10.6	-11.0
pcm1	56.2	39.1	-28.4	-23.0	-3.8	-5.3
cgcm3.1 t47	98.4	72.2	-15.3	-9.2	17.7	14.1
echo_g	21.7	12.8	-7.0	-4.5	1.3	0.4
ipsl_cm4	107.6	76.7	-30.5	-23.0	9.6	5.5
cnrm_cm3	21.5	13.0	-9.9	-4.9	-0.8	0.2
hadcm	29.1	18.2	-12.9	-8.0	-0.7	-0.5
miroc3.2	122.3	94.4	-13.6	-9.0	25.8	20.5

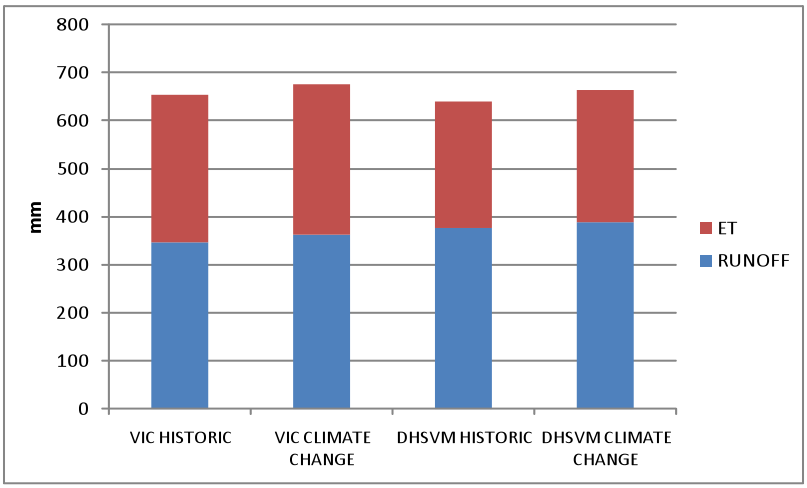

Figure 19 Total precipitation and partitioning into simulated runoff and evaporation for VIC and DHSVM for average historical conditions and the average of all climate change scenarios for the 2040s.

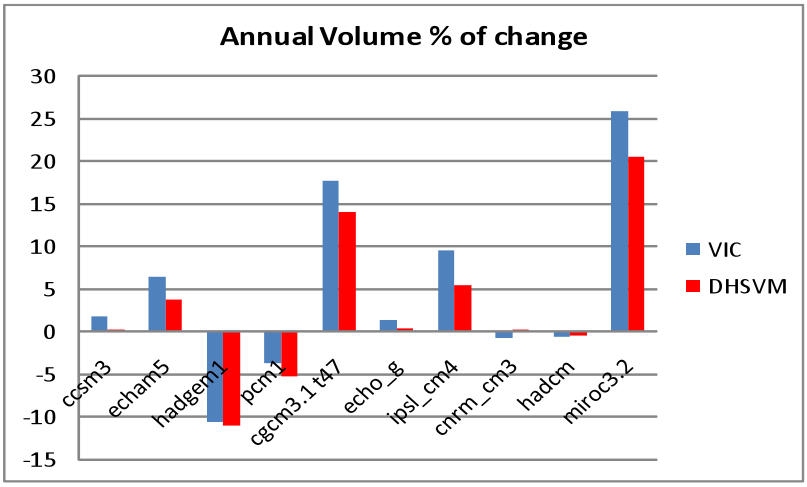

Figure 20 Changes in annual flow averaged over 10 climate change scenarios

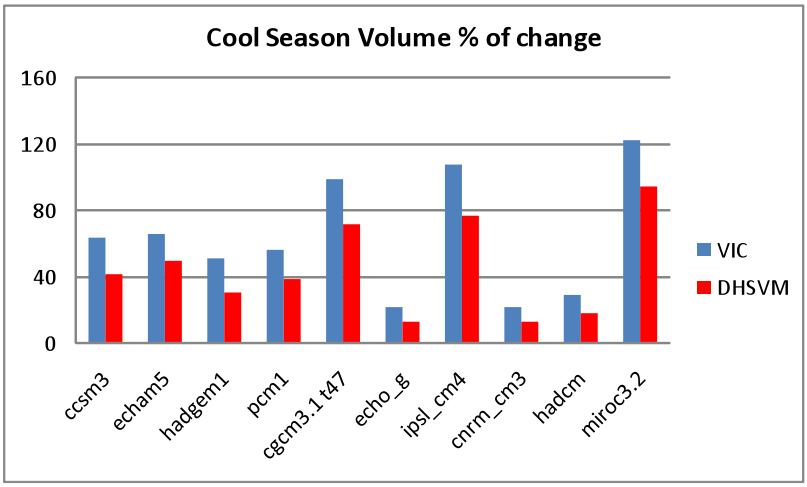

Figure 21 Changes in average cool season flow for 10 climate change scenarios

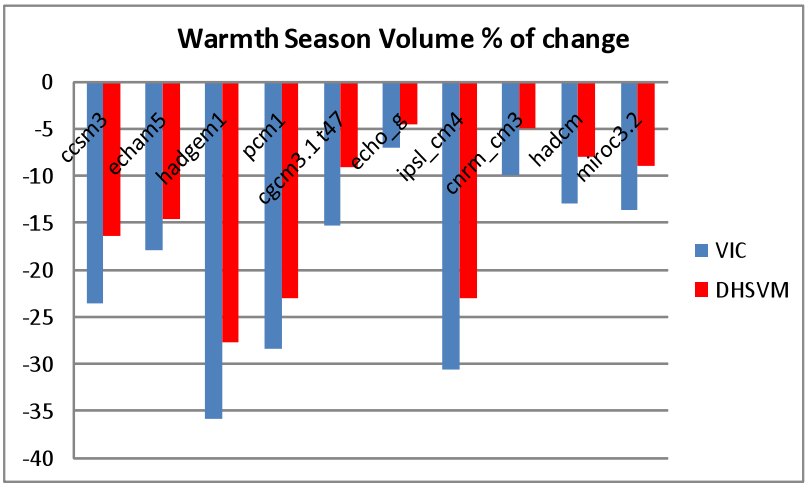

Figure 22 Changes in warm season flow for 10 climate change scenarios

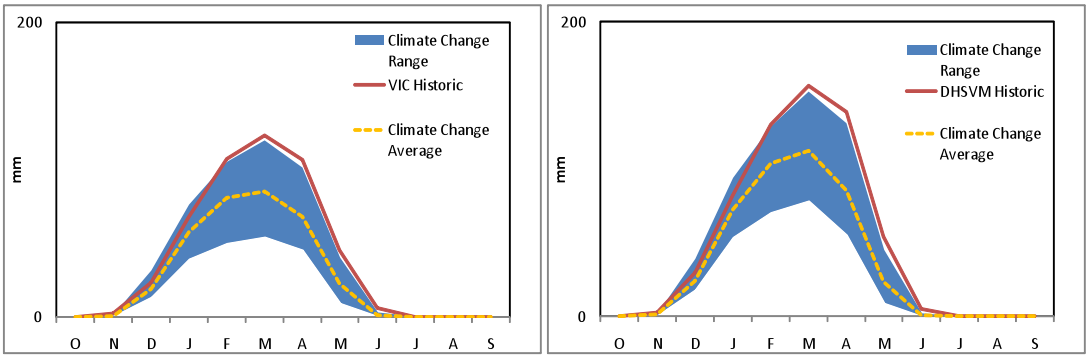

Figure 23 Snow water equivalent (millimeters) for historical conditions and 10 climate change scenarios simulated by VIC (left) and DHSVM (right).

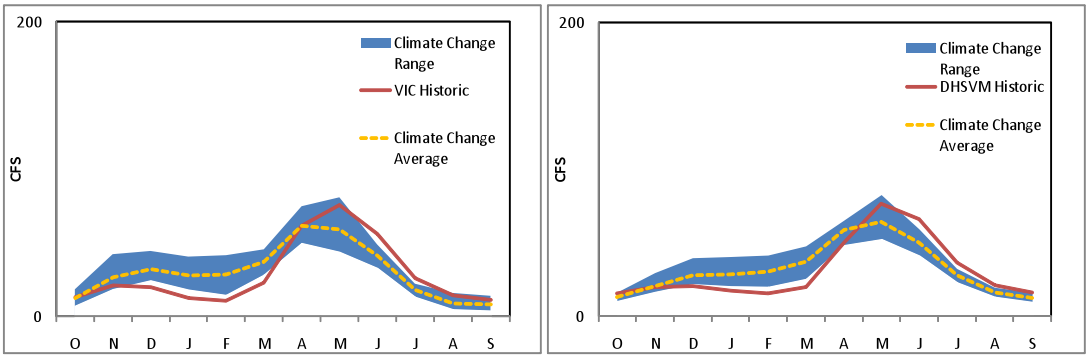

Figure 24 Streamflow (cubic feet/second) for historic and climate change time series.

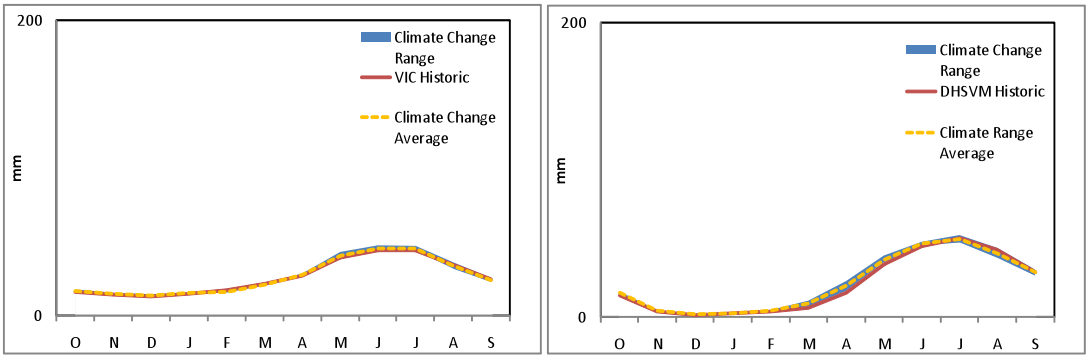

Figure 25 Evapotranspiration (millimeters) for historic and climate change time series.

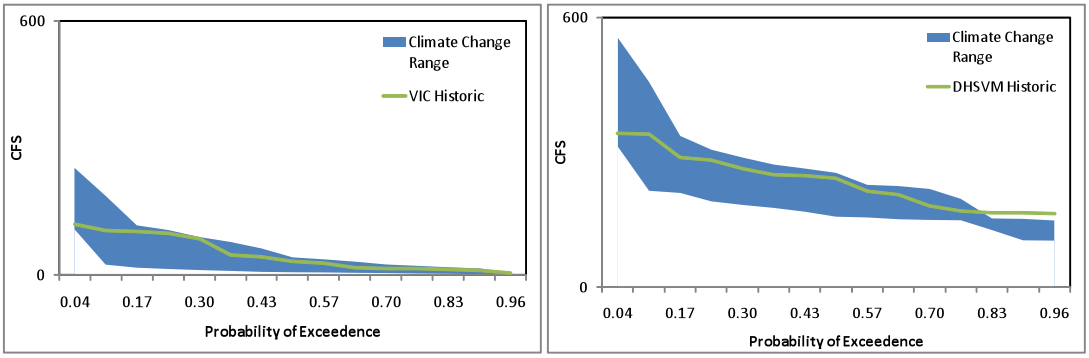

Figure 26 Quantiles for minimum 7 day average streamflow (cfs).

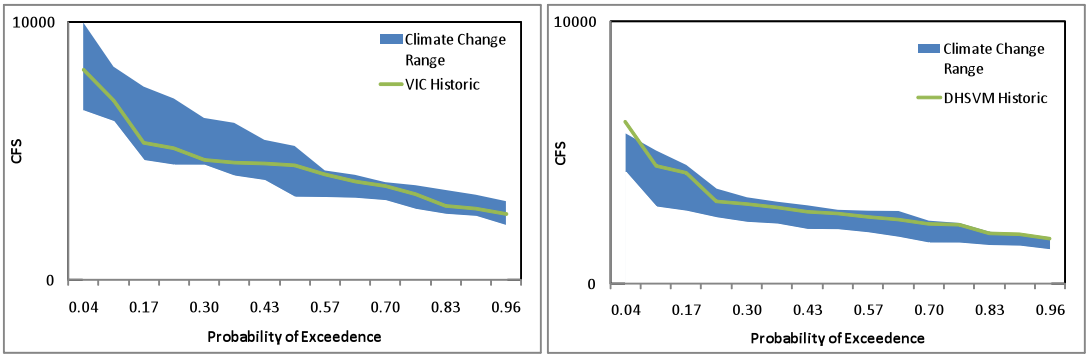

Figure 27 Quantiles for maximum streamflow (cfs).

4.2 Naches

Table 6 Change in streamflow for the climate change simulation expressed as a percent change with respect to the historical runs.

Naches						
Scenario	Cold Season % Change		Warmth Season % Change		Year % Change	
	VIC	DHSVM	VIC	DHSVM	VIC	DHSVM
ccsm3	48.5	29.8	-26.0	-25.3	-0.3	1.2
echam5	36.6	25.1	-13.1	-14.4	4.0	4.6
hadgem1	54.1	29.1	-45.6	-43.2	-11.3	-8.4
pcm1	36.4	21.6	-30.7	-30.7	-7.6	-5.5
cgcm3.1 t47	84.0	54.6	-17.1	-18.7	17.7	16.5
echo_g	29.7	18.9	-18.1	-18.4	-1.6	-0.5
ipsl_cm4	95.3	63.4	-16.8	-19.6	21.8	20.3
cnrm_cm3	44.3	33.3	-4.8	-8.6	12.1	11.6
hadcm	41.5	30.6	-9.7	-12.7	8.0	8.1
miroc3.2	102.4	66.7	-26.6	-28.0	17.8	17.5

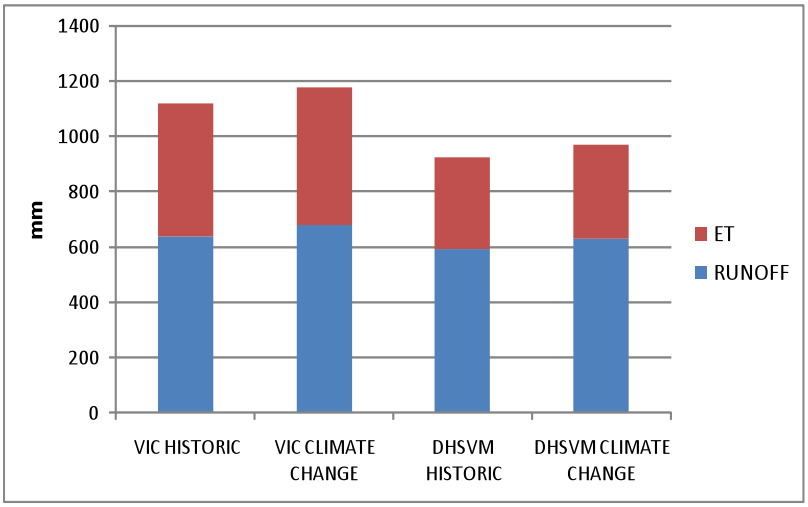

Figure 28 Runoff and precipitation for VIC and DHSVM historic and climate change average.

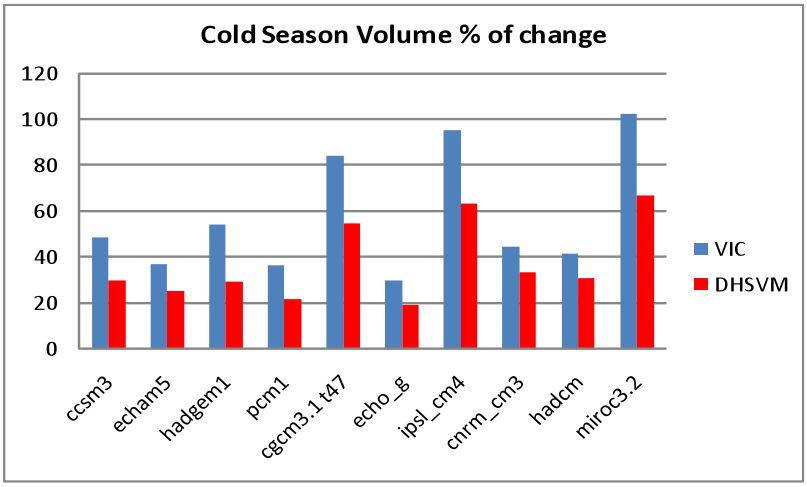

Figure 29 Percentage of change of total annual volume of water.

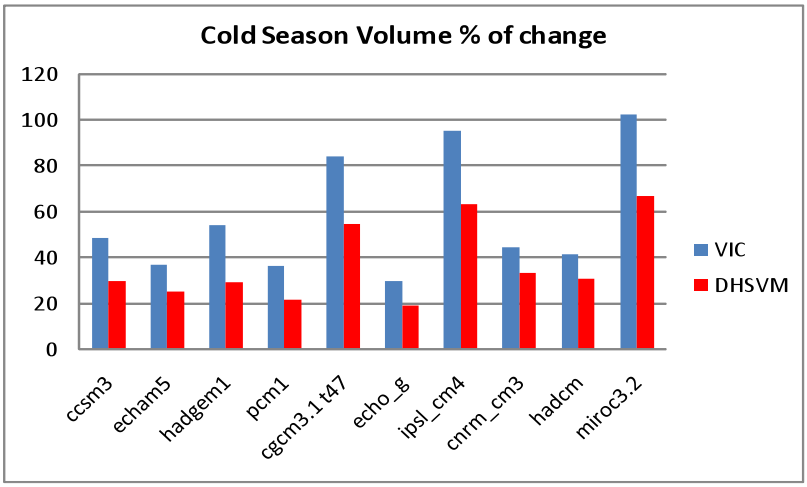

Figure 30 Percentage of change of cold season volume of water.

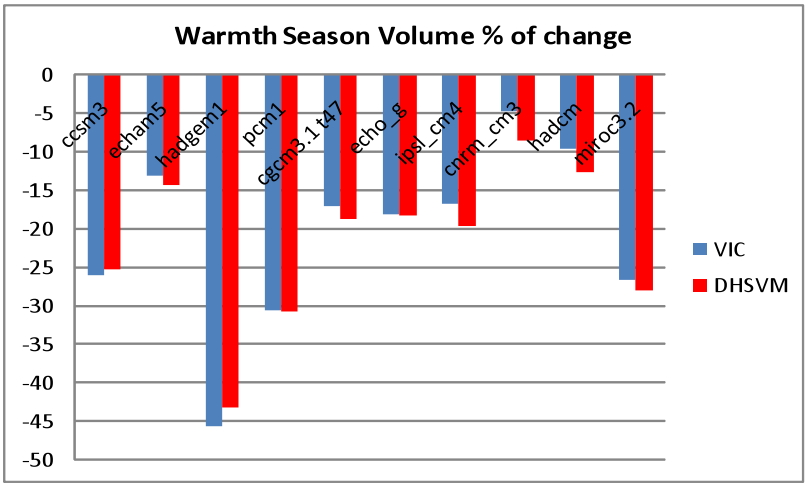

Figure 31 Percentage of change of the warmth season volume of water

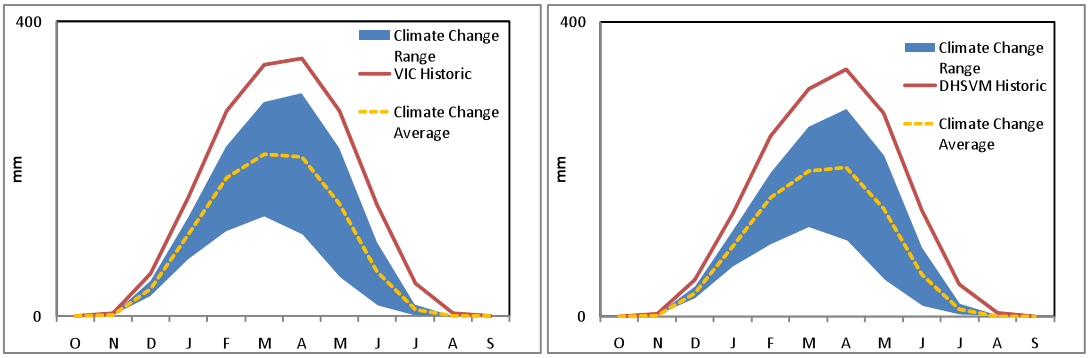

Figure 32 Snow water equivalent (millimeters) for historic and climate change time series, VIC and DHSVM.

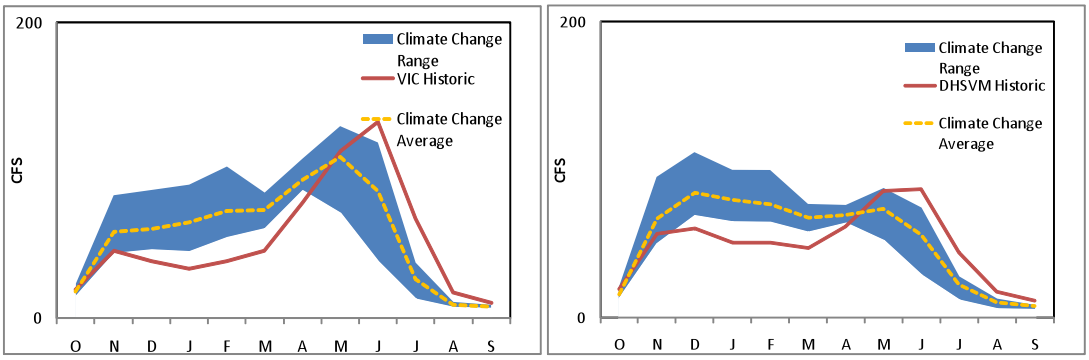

Figure 33 Streamflow (cfs) for historic and climate change time series.

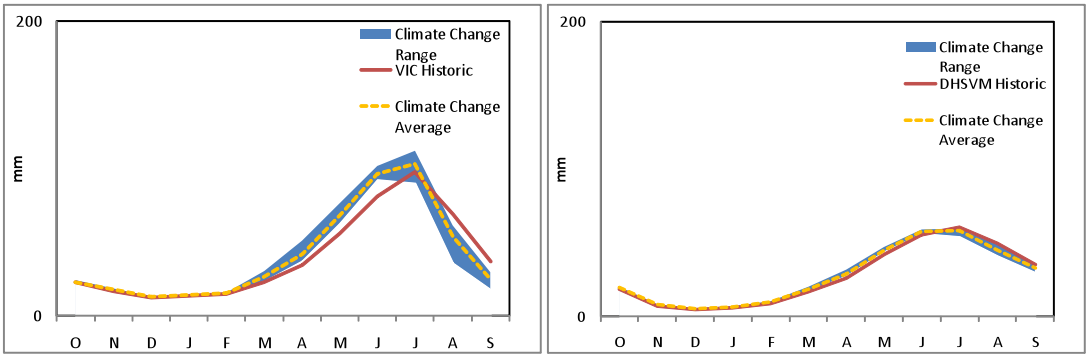

Figure 34 Evapotranspiration (millimeters) for historic and climate change time series.

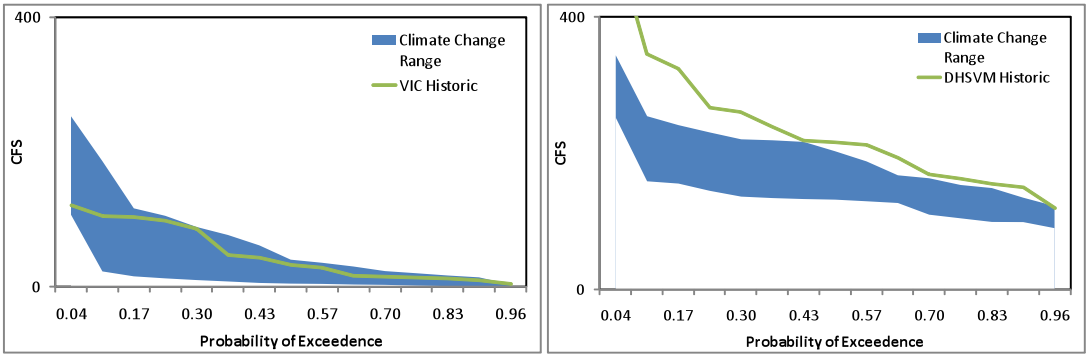

Figure 35 Quantiles for minimum 7 days streamflow (cfs).

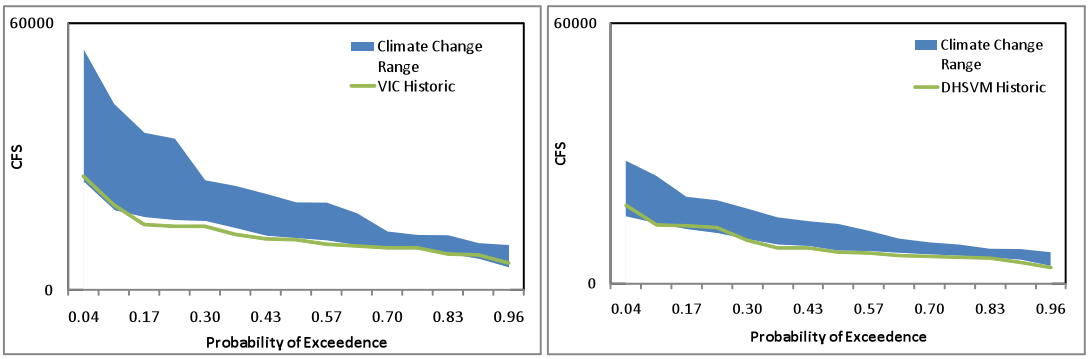

Figure 36 Quantiles for maximum streamflow (cfs).

4.3 Walla Walla

Table 7 Change in streamflow for the climate change simulation expressed as a percent change with respect to the historical runs.

Naches						
Scenario	Cold Season % Change		Warmth Season % Change		Year % Change	
	VIC	DHSVM	VIC	DHSVM	VIC	DHSVM
ccsm3	12.7	7.5	-7.1	-3.8	4.4	4.1
echam5	7.1	4.3	-11.8	-16.6	-0.8	-1.9
hadgem1	6.1	1.5	-14.8	-13.6	-2.7	-3.0
pcm1	-3.1	-7.0	-12.4	-12.1	-7.0	-8.6
ipsl_cm4	33.8	26.6	-11.6	-11.4	14.8	15.3
cnrm_cm3	21.2	19.1	4.4	8.2	14.2	15.8
hadcm	21.8	19.4	-7.7	-10.1	9.4	10.6
miroc3.2	36.9	29.4	-11.4	-10.7	16.7	17.4

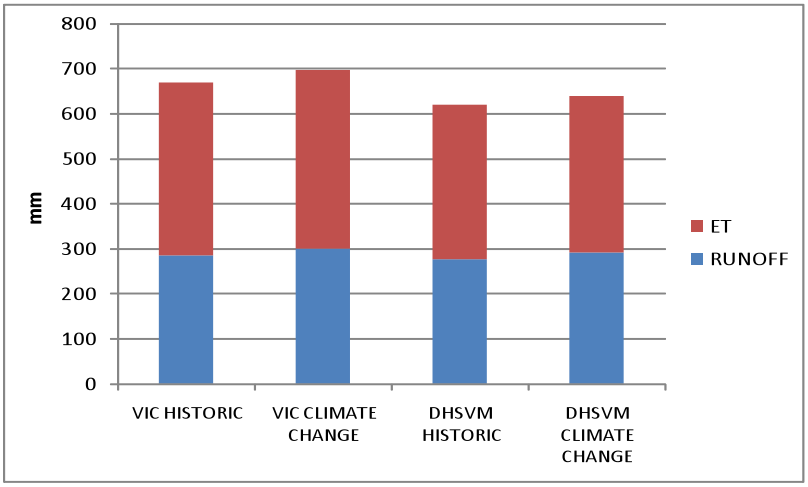

Figure 37 Runoff and precipitation for VIC and DHSVM historic and climate change average.

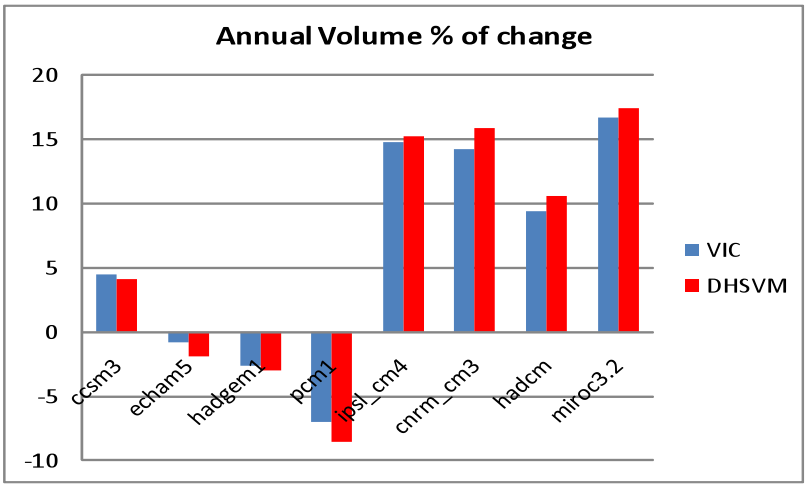

Figure 38 Percentage of change of total annual volume of water.

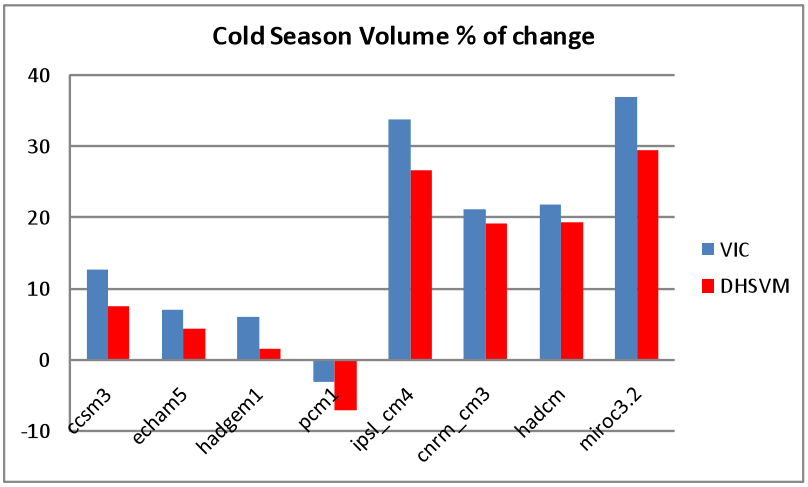

Figure 39 Percentage of change of cold season volume of water.

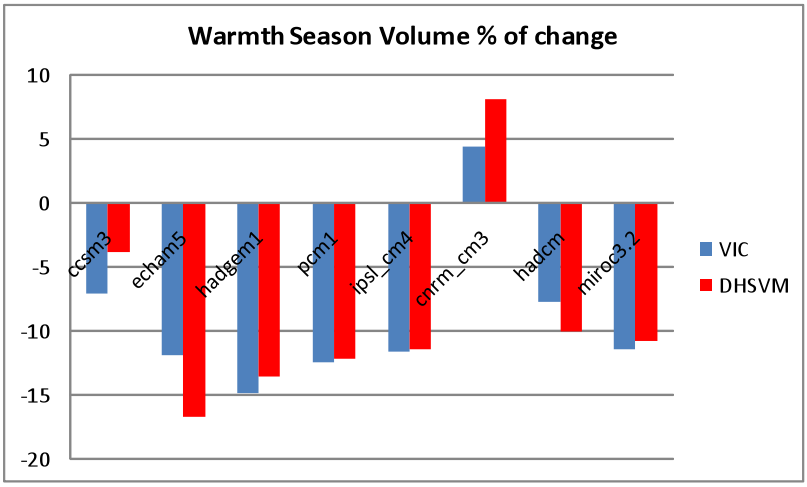

Figure 40 Percentage of change of the warmth season volume of water.

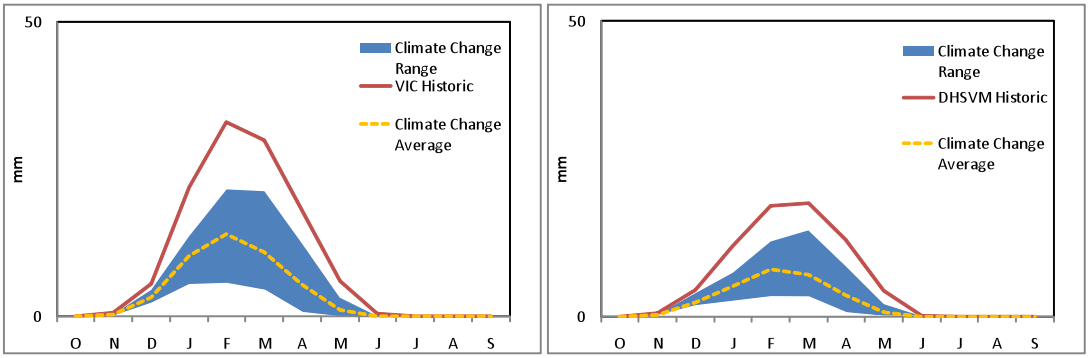

Figure 41 Snow water equivalent (millimeters) for historic and climate change time series, VIC and DHSVM.

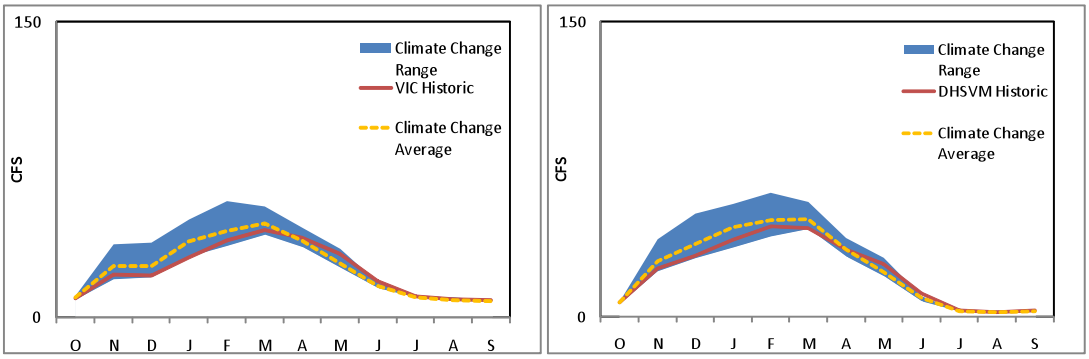

Figure 42 Streamflow (cfs) for historic and climate change time series.

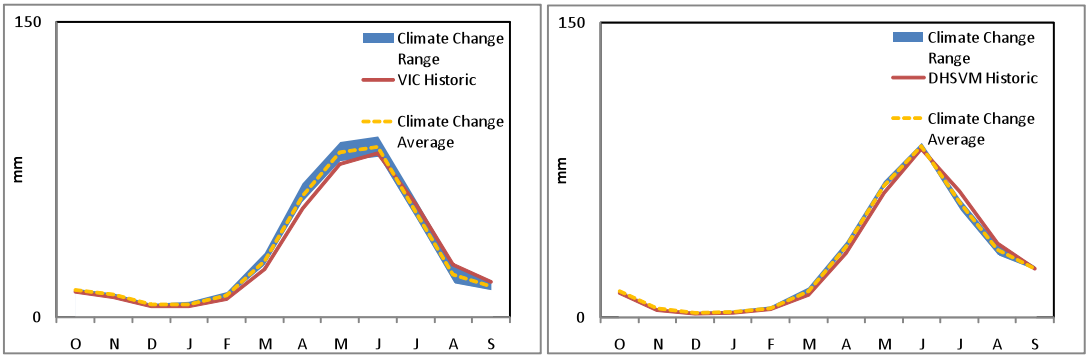

Figure 43 Evapotranspiration (millimeters) for historic and climate change time series.

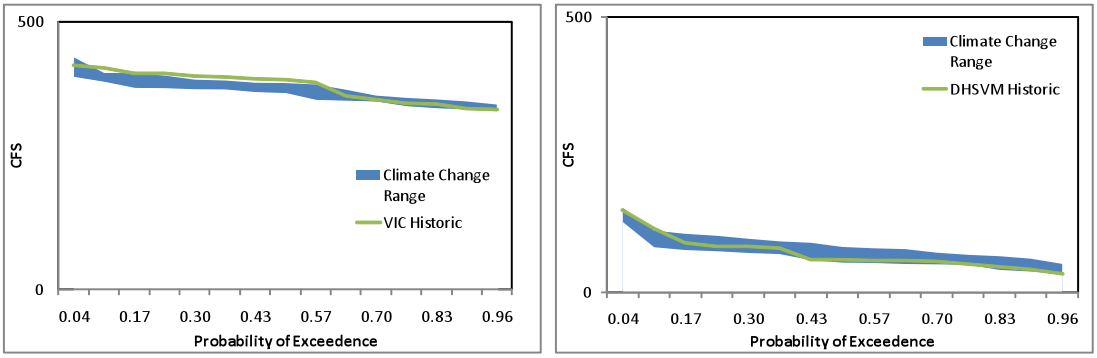

Figure 44 Quantiles for minimum 7 days streamflow (cfs).

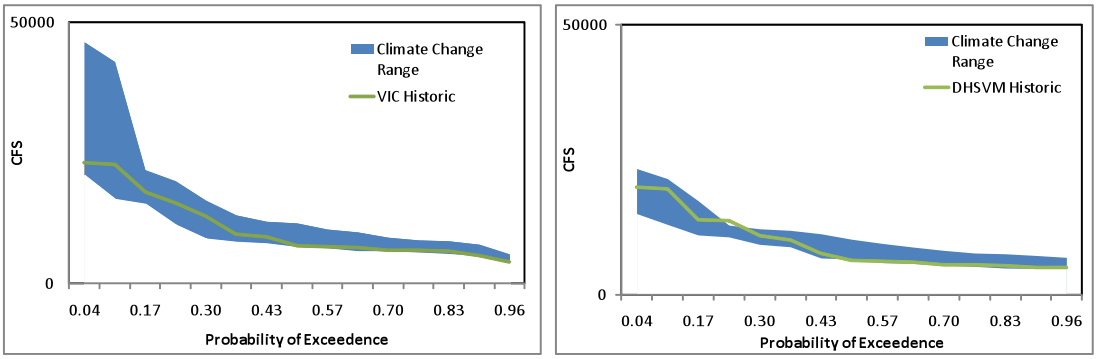

Figure 45 Quantiles for maximum streamflow (cfs).

4.4 Methow

Table 8 Change in streamflow for the climate change simulation expressed as a percent change with respect to the historical runs .

Methow						
Scenario	Cold Season % Change		Warmth Season % Change		Year % Change	
	VIC	DHSVM	VIC	DHSVM	VIC	DHSVM
ccsm3	42.7	52.2	-15.0	-28.9	1.5	-0.2
echam5	45.1	57.0	-7.2	-18.2	7.8	8.4
hadgem1	44.3	45.5	-27.7	-45.2	-7.1	-13.0
pcm1	38.6	44.0	-20.7	-37.1	-3.7	-8.3
cgcm3.1 t47	70.5	99.8	-3.9	-21.1	17.4	21.7
echo_g	19.1	24.8	-7.0	-14.0	0.5	-0.3
ipsl_cm4	83.2	110.3	-9.7	-29.6	16.9	20.0
cnrm_cm3	30.3	36.8	0.0	-4.4	8.7	10.2
hadcm	35.7	46.9	-2.6	-10.1	8.4	10.1
miroc3.2	97.2	133.5	-3.5	-22.3	25.3	33.0

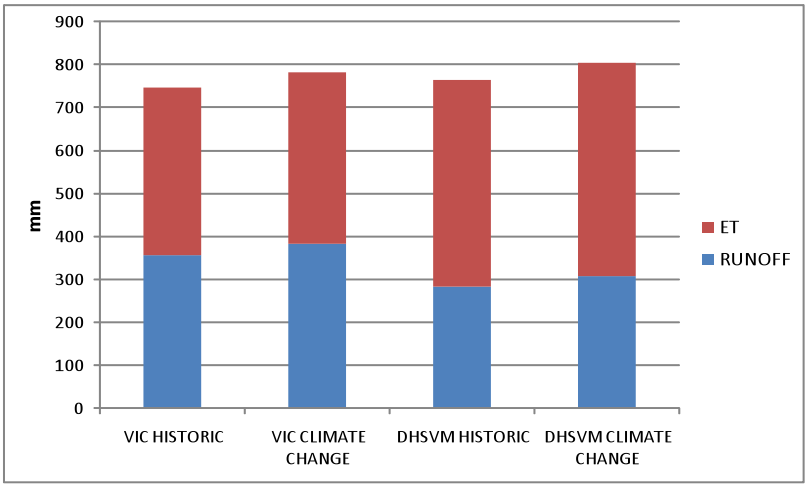

Figure 46 Runoff and precipitation for VIC and DHSVM historic and climate change average.

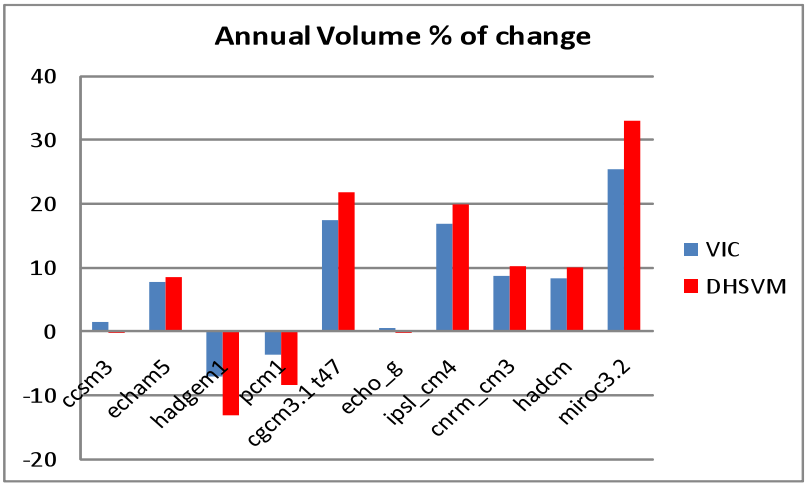

Figure 47 Percentage of change of total annual volume of water.

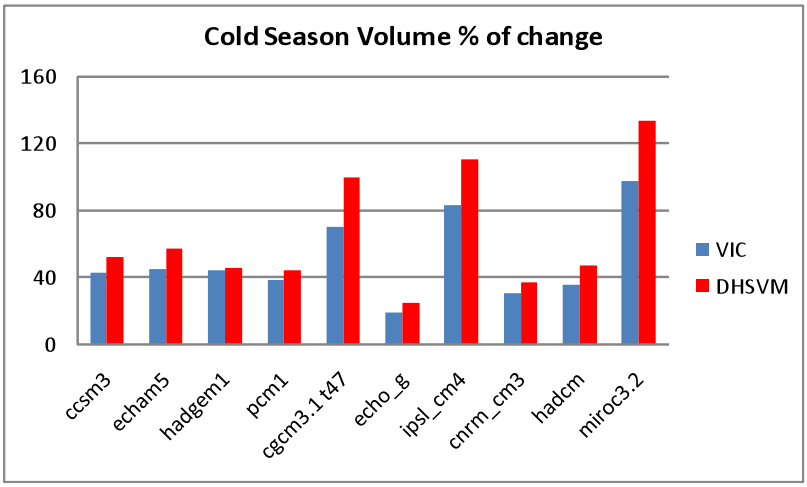

Figure 48 Percentage of change of cold season volume of water.

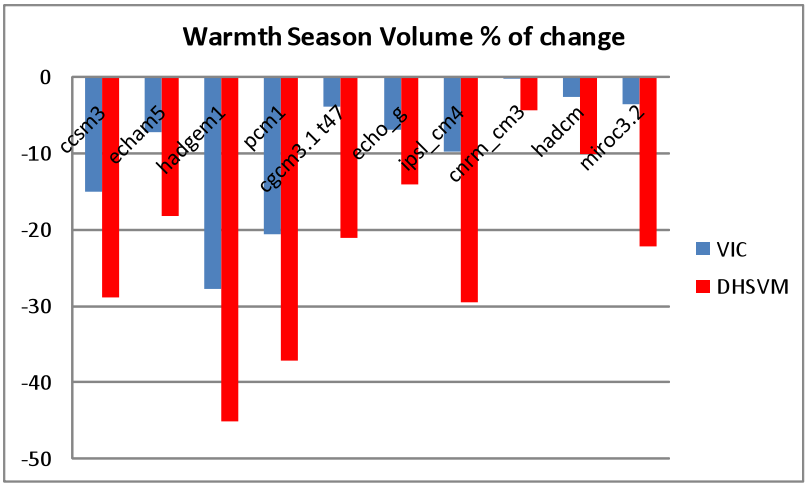

Figure 49 Percentage of change of the warmth season volume of water.

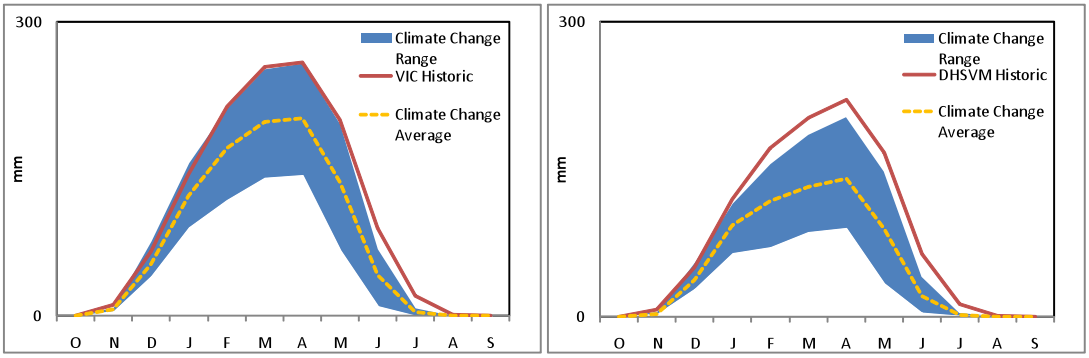

Figure 50 Snow water equivalent (millimeters) for historic and climate change time series, VIC and DHSVM.

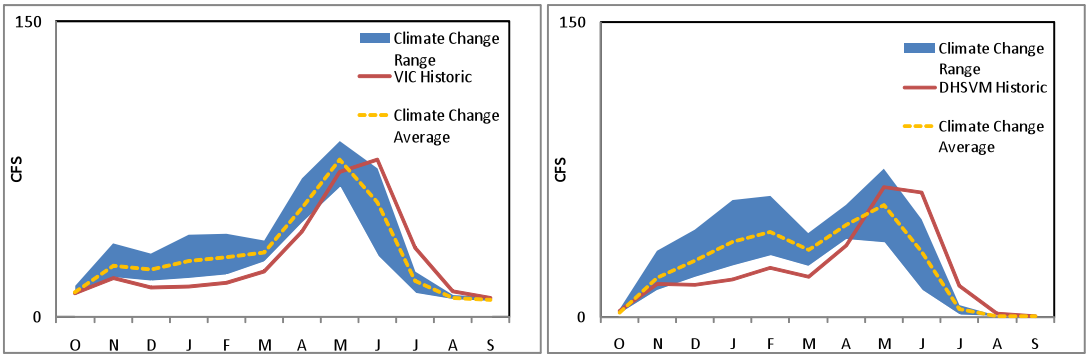

Figure 51 Streamflow (cfs) for historic and climate change time series.

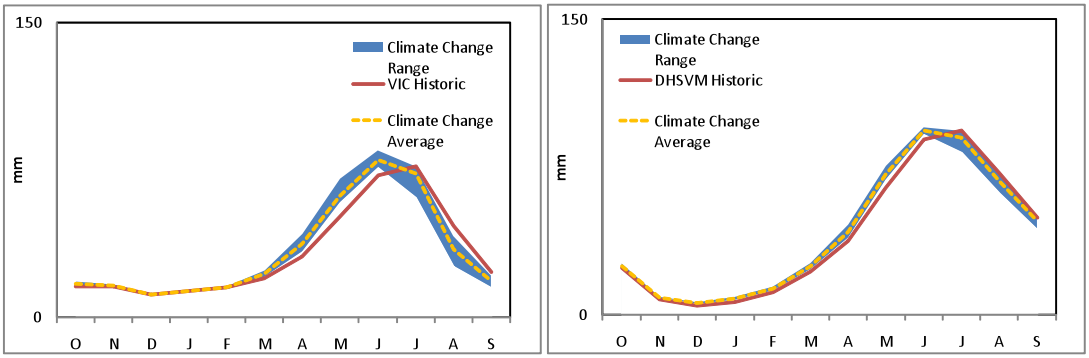

Figure 52 Evapotranspiration (millimeters) for historic and climate change time series.

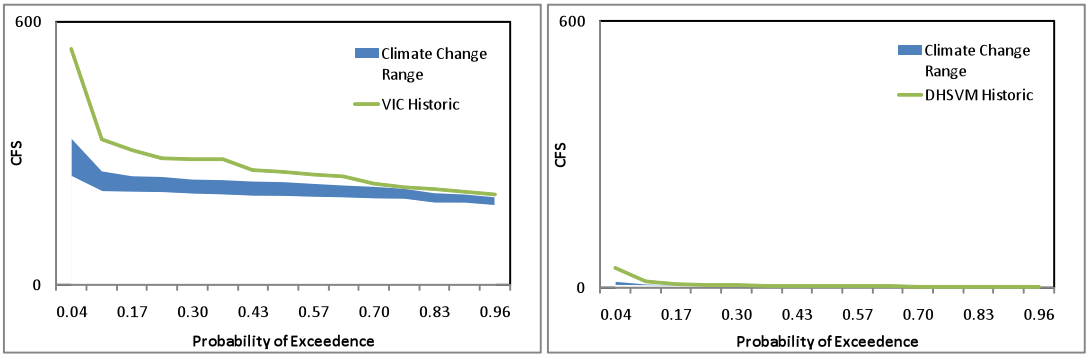

Figure 53 Quantiles for minimum 7 days streamflow (cfs).

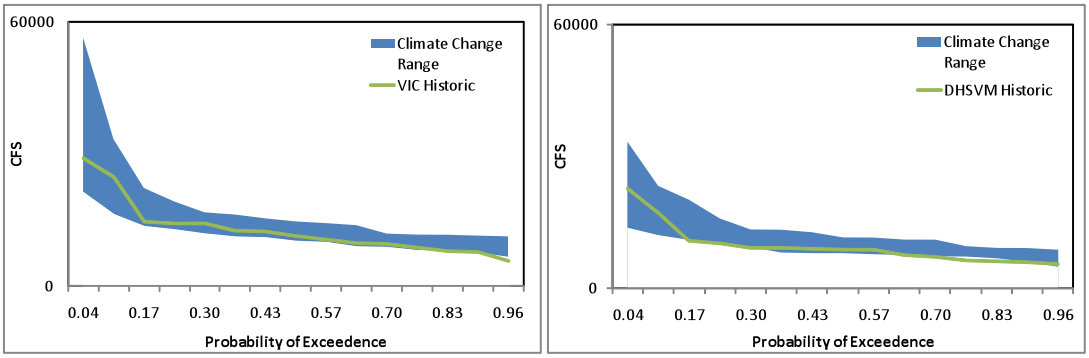

Figure 54 Quantiles for maximum streamflow (cfs).

4.5 Upper Yakima

Table 9 Change in streamflow for the climate change simulation expressed as a percent change with respect to the historical runs.

Upper Yakima						
Scenario	Cold Season % Change		Warmth Season % Change		Year % Change	
	VIC	DHSVM	VIC	DHSVM	VIC	DHSVM
ccsm3	43.6	35.9	-35.5	-35.8	-0.9	2.4
echam5	38.0	30.9	-22.4	-23.4	4.0	5.5
hadgem1	36.5	31.7	-54.3	-54.7	-14.6	-8.7
pcm1	31.2	26.7	-41.2	-42.1	-9.5	-5.5
cgcm3.1 t47	73.8	57.7	-31.6	-33.7	14.5	14.9
echo_g	27.4	23.4	-26.3	-26.5	-2.8	0.1
ipsl_cm4	82.2	65.3	-35.0	-37.4	16.3	17.3
cnrm_cm3	35.4	31.1	-12.7	-14.2	8.4	9.9
hadcm	35.4	31.8	-19.8	-21.1	4.3	7.1
miroc3.2	88.8	70.3	-40.3	-42.6	16.2	17.5

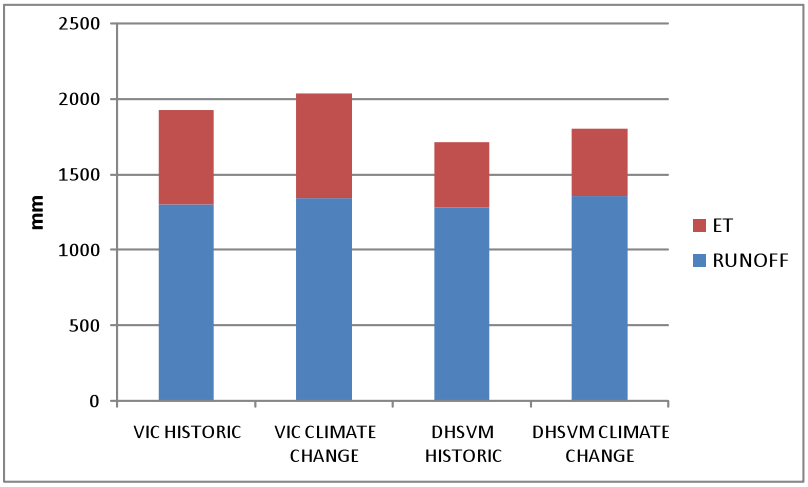

Figure 55 Runoff and precipitation for VIC and DHSVM historic and climate change average.

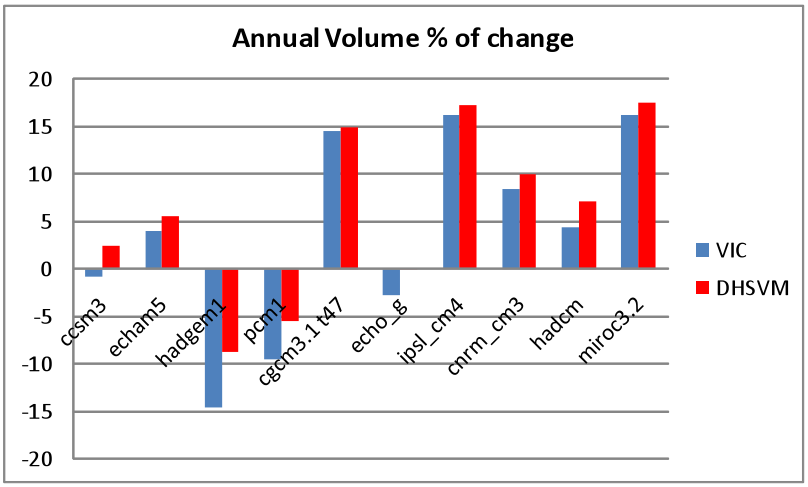

Figure 56 Percentage of change of total annual volume of water.

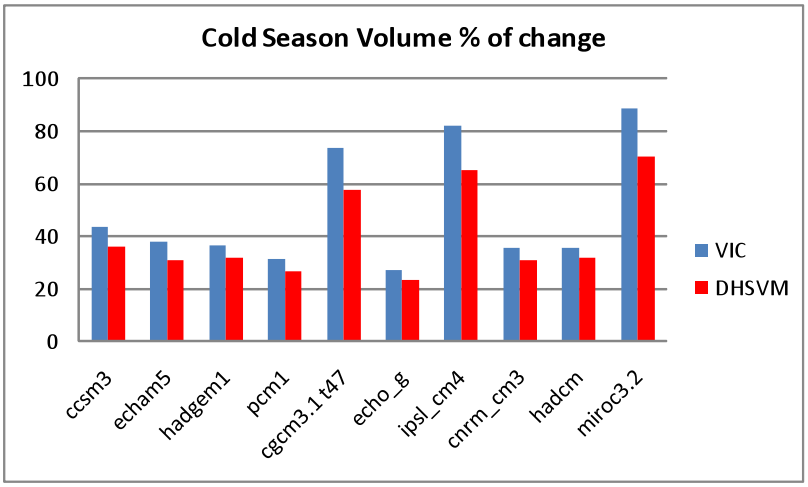

Figure 57 Percentage of change of cold season volume of water.

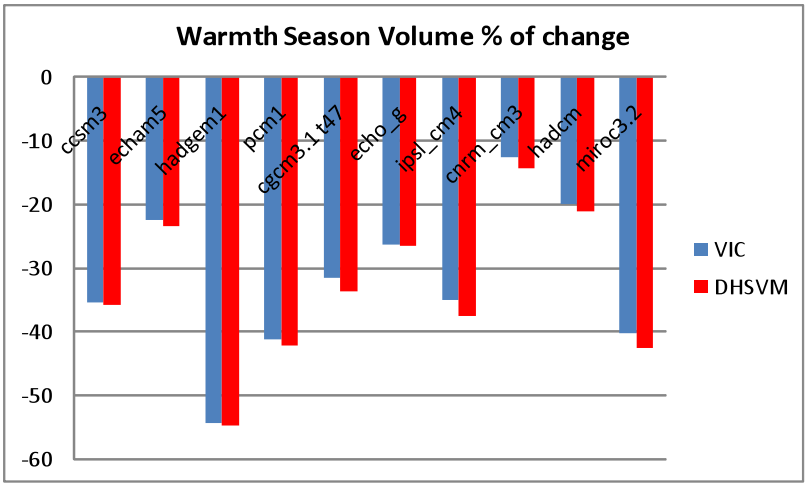

Figure 58 Percentage of change of the warmth season volume of water.

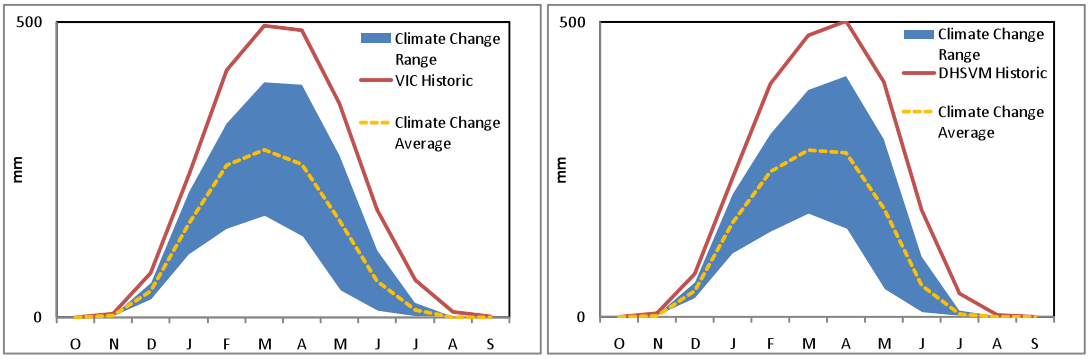

Figure 59 Snow water equivalent (millimeters) for historic and climate change time series, VIC and DHSVM.

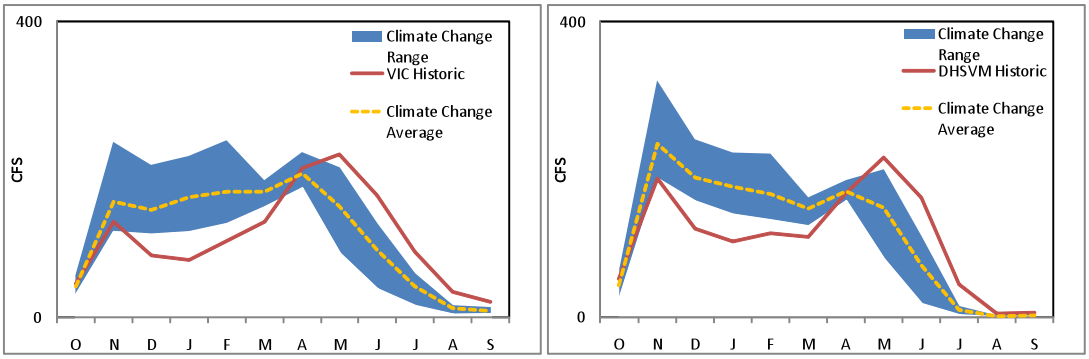

Figure 60 Streamflow (cfs) for historic and climate change time series.

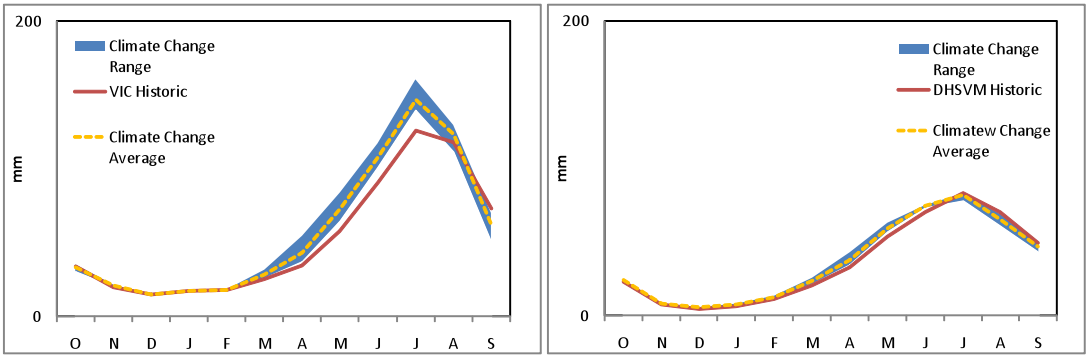

Figure 61 Evapotranspiration (millimeters) for historic and climate change time series.

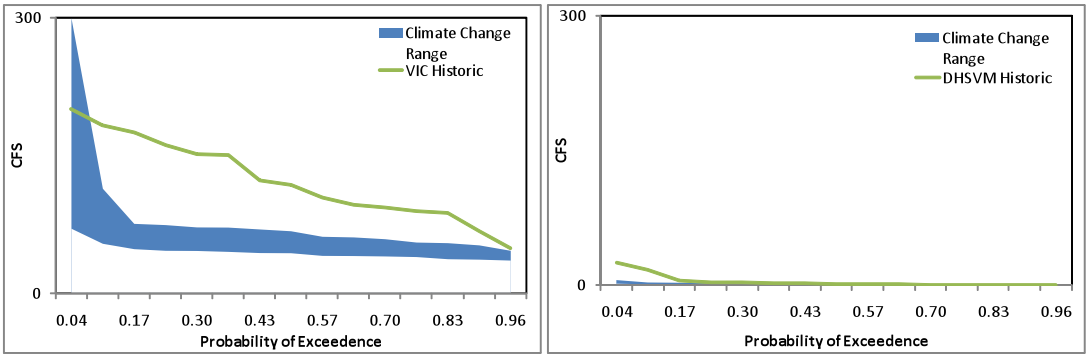

Figure 62 Quantiles for minimum 7 days streamflow (cfs).

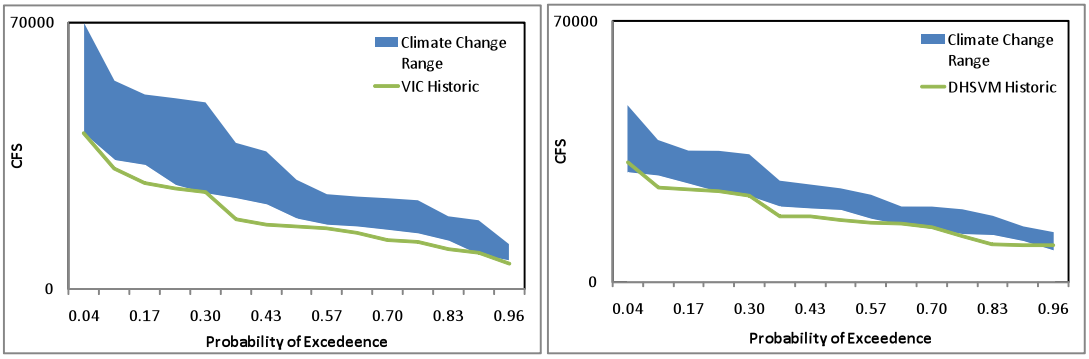

Figure 63 Quantiles for maximum streamflow (cfs).

5. Key Findings/Discussion

5.1 Implementation and Calibration

The main difference between DHSVM and VIC is that the first one is a complete distributed model and VIC is a macro-scale distributed model with some parameterization of runoff and baseflow processes. DHSVM requires a longer time to

implement, calibrate and run. However, it is capable of producing data at a resolution much finer than VIC. This output can be utilized to predict changes in small parts of the basin where VIC resolution is too coarse. Both models require essentially the same data to be implemented; however, the resolution at which this data is required and utilized is different, and there are additional parameters for DHSVM.

The calibration process for the two models is similar. In this step, soil parameters are adjusted to produce a hydrograph similar to the observed streamflow. Nevertheless, the process is more efficient in VIC since running the model takes less time. In this study DHSVM was configured to use the same input parameters as VIC. In particular, the groundwater model in DHSVM was deactivated as a way to make the baseflow estimation and soil storage capacities more comparable. The absence of this component produces some extremely low values during summer time in some basins. Our primary reason for this selection was to investigate the differences in climate sensitivity when simulating fine scale processes explicitly using a high resolution model, in comparison with a macro-scale approach using VIC. The incorporation of deep ground water in DHSVM implementation, although it might improve baseflow simulation, confounds this aspect of the comparison.

5.2 Results

The results illustrate that both models predict the same qualitative effects of climate change for snow accumulation and melt statistics, evapotranspiration and streamflow. However, some significant differences in model sensitivity are apparent. In most of the basins VIC produces more streamflow during the warm season than DHSVM. This discrepancy is due to the fact that DHSVM groundwater module was turned off and only soil drainage was used to generate baseflow, significantly reducing base flow generation during the warm season for DHSVM.

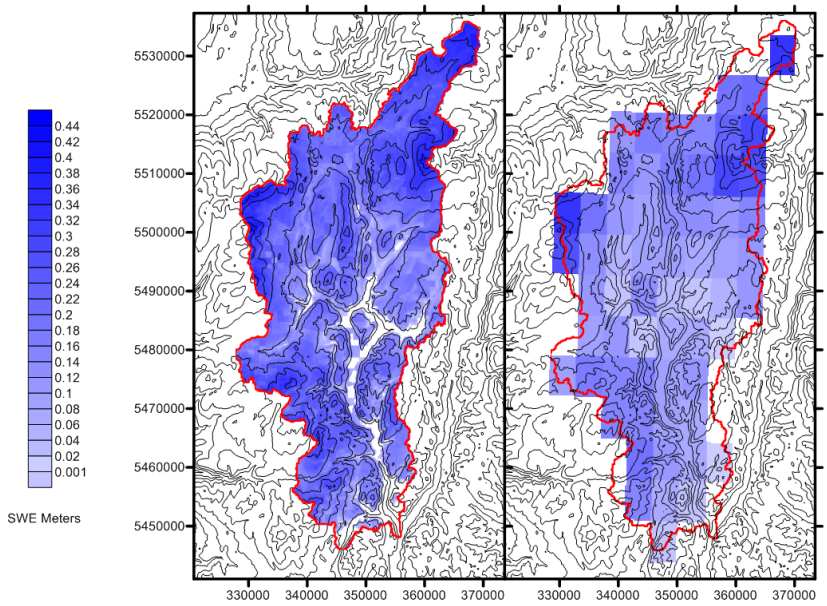

Figure 64 Comparison between SWE generated by DHSVM (left) and VIC (right).

In Figure 64, VIC and the DHSVM snow water equivalent (SWE) is compared in the West Kettle Basin. The DHSVM image (left map) is composed of 84,814 cells while the one generated by VIC (right map) uses only 62 cells. The finer resolution utilized in DHSVM is better able to represent the absence of snow in the bottom of the valleys and greater accumulations at high elevations zones. Furthermore, the detailed representation of vegetation at the same resolution as the DEM is able to correctly associate SWE with different vegetation canopy conditions. Although in the case of the Kettle, DHSVM simulates greater SWE than VIC. This pattern is not repeated in other basins and there seems to be no clear relationship between model formulation and relative amounts of SWE. This result suggests that these factors are emerging as a result of the complex interplay between model resolution, model processes and physics, and calibration effects, but that spatial resolution does not dominate these interactions.

The implementation of DHSVM and VIC are similar in the number of GIS layers required. However, the preprocessing of those layers of information is different. In VIC the data is aggregated to mean values of parameters according to the resolution of the model. On the other hand, DHSVM's finer spatial resolution allows data to be more

accurately represented at their geographic location. This characteristic allows DHSVM to more accurately represent outputs like SWE or ET for ecological studies at relatively fine spatial scales.

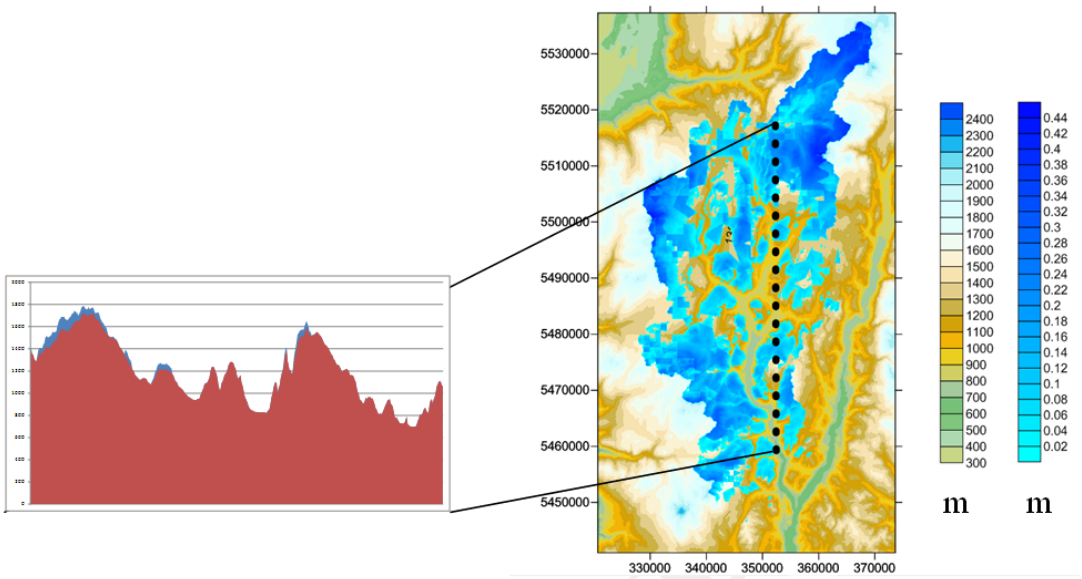

Figure 65 Transect of topography and amount of SWE generated by DHSVM.

Figure 65 shows a transect section of the West Kettle basin elevation and SWE estimation for May 1 1996 generated by DHSVM. The graph at the left shows that snow accumulation is higher in the north facing slopes than in the south facing. This trend is attributable to the ability of DHSVM to simulate the sky percentage of each cell and topographic shading, both of which affect incoming solar radiation during the day. Therefore, more short wave energy reaches south facing cells than those facing north. The VIC model is not able to simulate this difference and all the area contained in a cell is exposed to the same amount of energy. These physical processes are important for studies related to vegetation disturbance and recovery, for example.

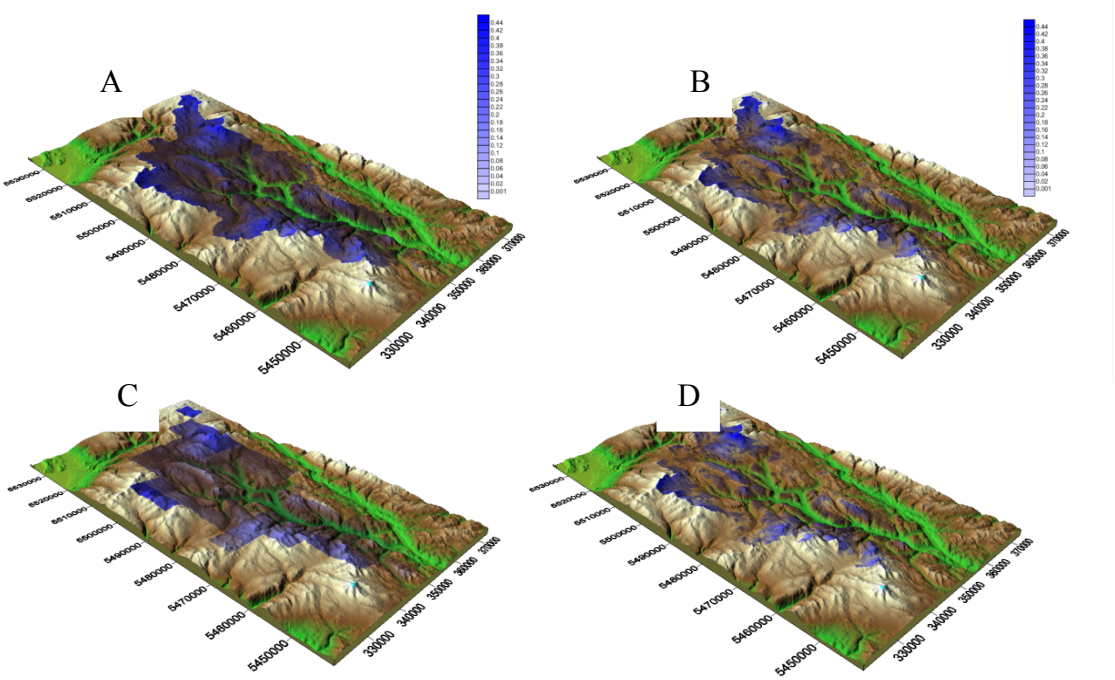

Figure 66 Panel A presents SWE as April 1 1996, Panel B presents SWE for May 1 1996, Panel C presents SWE for VIC during April 1 1996 and for Panel D presents SWE for DHSVM using the MirocA1B scenario for the period 2030-2059 during April 1 1996

Figure 66 shows SWE estimates for the West Kettle Basin in four conditions. Panel A shows the prediction of DHSVM for April 1, 1996. Panel B illustrates DHSVM for May 1 of the same year. Panel C indicates the VIC estimate of SWE for April 1, 1996; and finally, panel D shows the DHSVM SWE estimate for April 1, 1996 utilizing the meteorological files downscaled from the global climate model MIROC3.2 (see Chapter 4, this report).

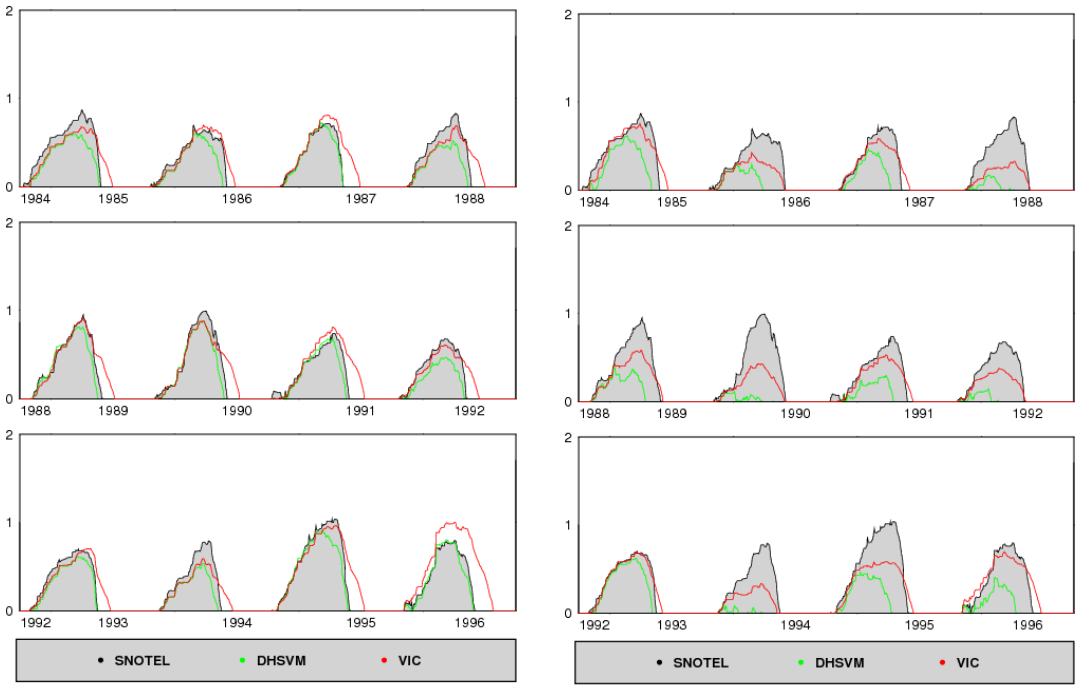

Figure 67 SWE (meters) at Sasse Ridge SNOTEL for Historical (left) and MIROC3.2 (right) meteorological data sets

Figure 67 plots SWE at Sasse Ridge SNOTEL resulting from the DHSVM and VIC model. The left panel presents historic data; here for most of the years the SWE is similar for both models and shows an excellent agreement with the peak quantity in the observed data. However, the melting process seems to be slower in VIC and therefore it is predicting higher amounts of SWE during spring. This slower melting process can be generated by a smaller amount of energy reaching the basin and the fact that VIC utilizes bigger cells where the elevation represents on average a larger area than DHSVM. It is import to note that in this case the results for DHSVM represent the average of a 150 x 150 m cell. In contrast, in the VIC model the results are the average of a 6000 x 6000 m cell. The right panel of figure 67 presents the same observations of SWE in the background and the predictions of DHSVM and VIC utilizing meteorological forcing of the MIROC3.2 GCM. Here again, VIC is generating more SWE and melting slower than DHSVM. This shows that DHSVM SWE predictions react with a higher sensitivity to the climate change scenarios. One of the reasons of this higher sensitivity is the difference in resolution of the cells and a more detailed DHSVM representation of the elevation (and therefore temperature) and vegetation in each of these cells.

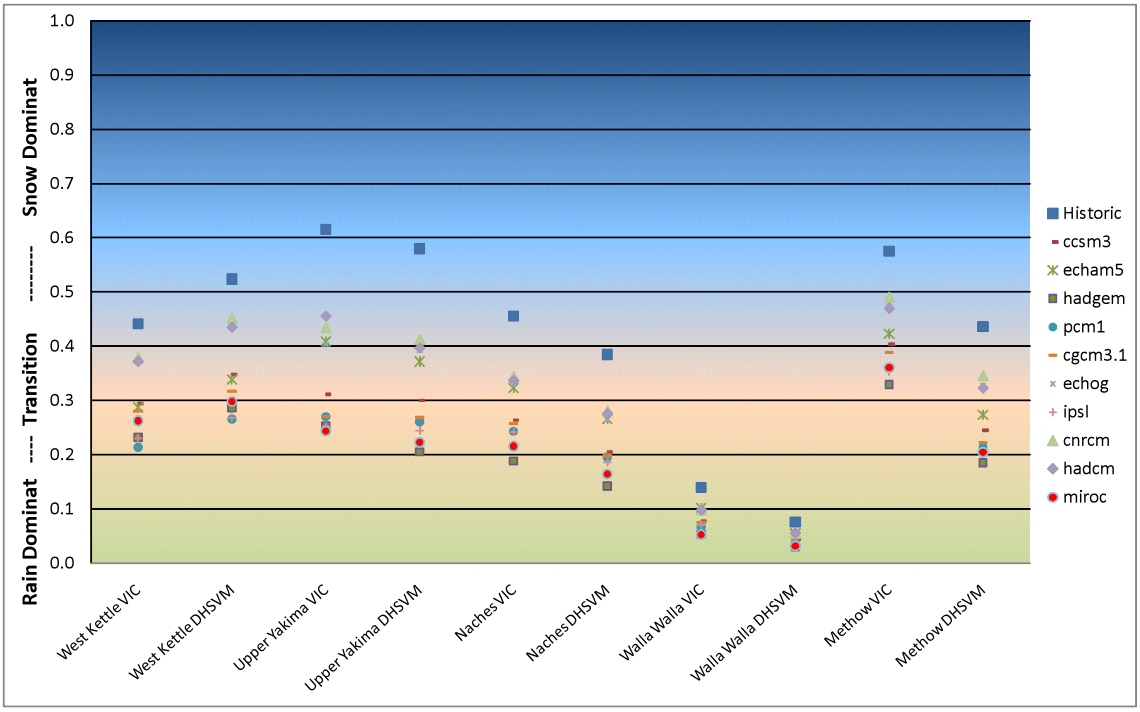

Figure 68 Ratio of Peak SWE to October-March precipitation

Figure 68 presents information about the ratio of peak SWE to October-to-March precipitation for the five basins, the two hydrologic models and all the meteorological forcing. This ratio is utilized to categorize basins as either rain dominant, where most of the precipitation is rain; transition, where there is a mix of snow and rain; or, snow dominant, where most of the annual precipitation is snow during the cool season (Elsner *et al.* 2010). As general rule, watersheds in the headwaters of the basins are classified as snow dominant, while lower elevation watersheds are classified as rain dominant. Mid-elevation basins are normally classified as transient watersheds. These are particularly sensitive to climate change because small perturbations in temperature can significantly change the amount of precipitation falling as snow over relatively large areas. In the five basins analyzed both models predict similar percentage of change. Also, both models predict an equal shift in basin categorization. For example, in the Upper Yakima Basin both hydrologic models classify the basin as snow dominant when historic data is used. Meanwhile, when climate change meteorological files are used both hydrologic models also predict a change to a transition basin.

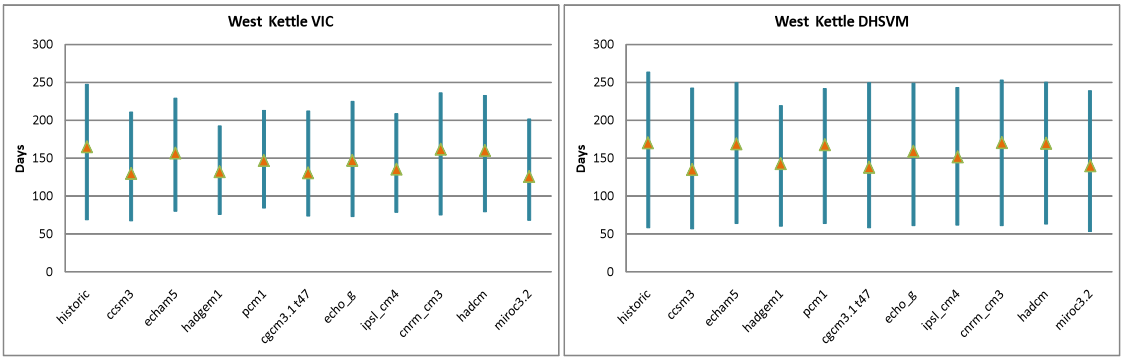

Figure 69 Day of 10%, Max and 90% of SWE for VIC and DHSVM in West Kettle River Basin

Figure 69 presents data for the day of 10% SWE accumulation, day of peak SWE and day of 90% melting of SWE for the West Kettle River Basin using VIC (upper panel) and DHSVM (lower panel). The blue line represents the length in days from 10% of accumulated SWE to the day of 90% melting. The day of peak SWE is represented by a yellow triangle. The graphic shows that for this basin both models predict similar behavior in modeling the day of 10% of peak SWE and the day peak SWE, the main difference is in the day of 90% of melting. The reason for these differences is the higher resolution of the cells and the application of temperature lapse rates in DHSVM. Also, the high percentage of cells facing north results in reduced melting rates due to the lower shortwave radiation generated by the topography shadowing. Finally, there are also differences in the canopy interception model and SWE calibration process related to canopy closure.

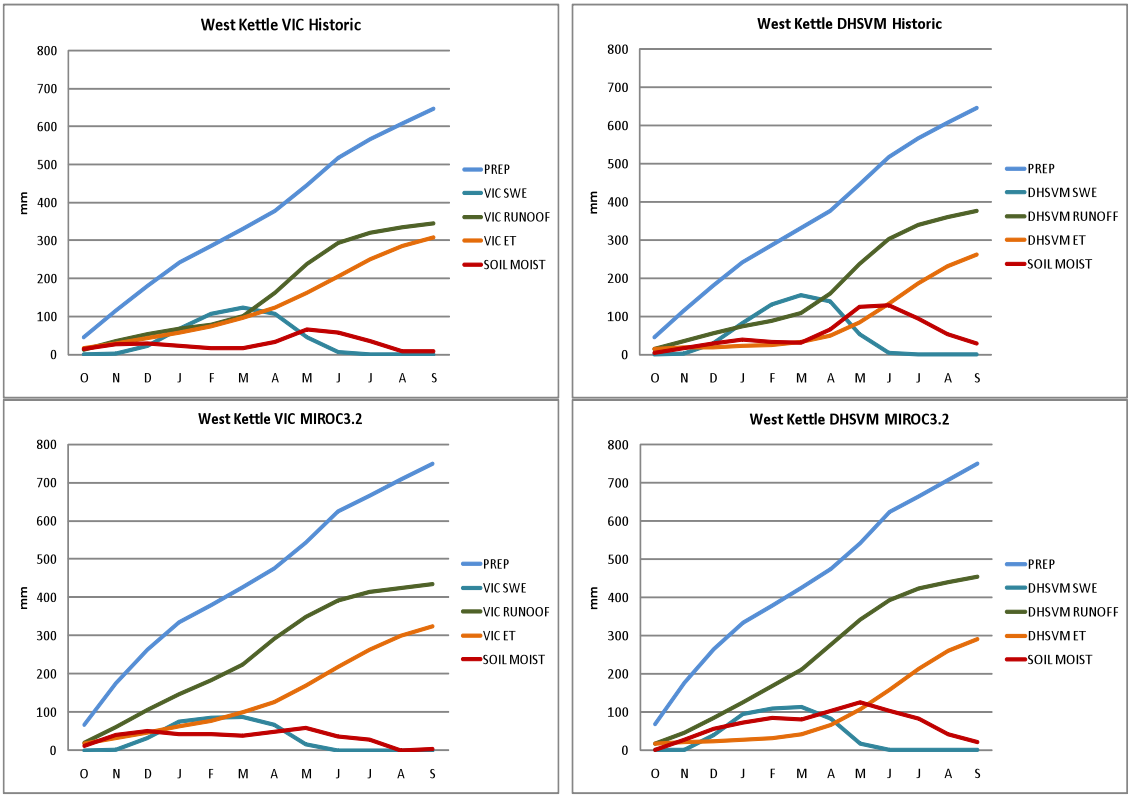

Figure 70 Cumulative Precipitation, ET, Runoff, Soil Moisture, and SWE for the W. Kettle Basin. (Note that residual soil moisture is subtracted from the total soil moisture in the plots to show the seasonal cycle.)

Figure 70 presents cumulative precipitation, runoff and ET for the West Kettle Basin. The top two panels are mean values for the historic data (1985 to 2000) estimated by VIC and DHSVM, respectively. Bottom panels plot the mean value for the same period utilizing the MIROC3.2 meteorological data set. In the case of the historic data set VIC is generating 8.9 less runoff and 15% more ET than DHSVM. The MIROC3.2 represents an increase in precipitation of 16% over the basin. Under this scenario VIC shows an increase of 25% in runoff and in DHSVM the increase is 21%. The differences between them are 4.6% less runoff and 10% less ET in VIC than in DHSVM when MIROC3.2 meteorological files are used.

5.3 Computation and Storage

One final comparison is the time required to run the models and the storage required. Since VIC resolution is much lower, the running time are considerable shorter.

One of the main differences in the outputs for streamflow calculations is that VIC requires outputs for each cell while DHSVM does not. However, when special analyses are required, the storage required by DHSVM can easily become overwhelming due to the number of pixels.

6. Summary and Conclusions

The VIC macroscale hydrologic model and the DHSVM were compared in five basins of the PNW. The VIC model was implemented at $1/16^{th}$ degree spatial resolution and DHSVM at 150 m over the historical period 1985-2000 and projected climate change scenarios. Climate change scenarios were based on the hybrid delta meteorological downscaling for 10 global climate models for the A1B greenhouse gas emissions during the time period of 2030 to 2059.

In general, both models predict the same qualitative changes in key water balance variables due to climate change. Both models, for example, showed reductions in SWE, increased cool season streamflow, decreased warm season streamflow, and consistent changes in the sign and approximate magnitude of annual flows and hydrologic extremes. The sensitivity of each model to the combined effects of warming and precipitation change, however, is often substantially different in absolute terms.

In some isolated cases (e.g. in the case of rates of snow melt at particular SNOTEL sites—see Figure 67), it is possible to show that DHSVM is probably better than VIC at representing a physical process to which the outcomes are sensitive. However, in most cases only the differences in sensitivity between the two models result from hydrologic modeling uncertainty arising from multiple sources that are not easily isolated. Thus, although the models in some cases show substantially different sensitivity to climate, it is difficult to conclude that one or the other is demonstrably better at reproducing the actual (and generally unmeasured) sensitivity.

Although differences are apparent between the two models, it appears that the only clear advantage to using DHSVM at these high spatial resolutions is for watersheds where spatial variation in solar radiation is an important driver of study outcomes. An example would be vegetation studies where important differences are apparent on north and south facing slopes resulting from differences in water availability or other factors. In such cases, the finer resolution of the DHSVM and the inclusion of processes that determine variations in radiation with slope and aspect allow it to produce more detailed information essential for such studies.

For water resources studies where streamflow is the primary outcome of interest, uncertainties due to hydrologic model formulation are potentially relevant. However, uncertainties in temperature and precipitation projections are probably an equally important, or more important, source of uncertainty. Furthermore, investigating alternative macro-scale hydrologic modeling formulations (e.g. following Clark *et al.* 2008) would probably be a less computationally intensive way to explore the role of hydrologic modeling uncertainty on outcomes, as opposed to implementing fine scale hydrologic models.

7. References

Andreadis, K., P. Storck, and D. P. Lettenmaier (2009) *Modeling snow accumulation and ablation processes in forested environments,* Water Resources Research, 45, W05429, doi:10.1029/2008WR007042.

Arya, S. Pal (1998) *Introduction to Micrometeorology*. San Diego: Academic Press.

Brooks, R.J., and A.T. Corey (1964) *Hydraulic properties of porous media*. Hydrol. Pap. 3. Colorado State Univ.: Fort Collins; 27.

Chapra, S. C. (1997) Surface Water-Quality Modeling. Surface Water-Quality Modeling. McGraw-Hill.

Clark, M.P., Slater, A.G., Rupp, D.E., et al. (2008) Framework for Understanding Structural Errors (FUSE): A modular framework to diagnose differences between hydrological models, WRR, 44, W00B02

Doten, C.O. and D.P. Lettenmaier (2004) *Prediction of sediment erosion and transport with the Distributed Hydrology-Soil-Vegetation Model*. Water Resources Series Technical Report Number 178. U. Washington: Seattle; 63.

Dickinson, R.E., A. Henderson-Sellers, and P.J. Kennedy (1993) *Biosphere-Atmosphere Transfer Scheme (BATS) Version 1e as Coupled to the NCAR Community Climate Model: NCAR Technical Note*, NCAR/TN-387+STR. National Center for Atmospheric Research: Boulder, CO; 72

Eagleson, P.S, (1978) *A simplified model of soil moisture movement in liquid phase*, Water Resources Research, 14(5), 722-730

Elsner, M.M., L. Cuo, N. Voisin, J.S. Deems, A.F. Hamlet, J.A. Vano, K.E.B. Mickelson, S.Y. Lee, D.P. Lettenmaier (2010) *Implications of 21st century climate change for the hydrology of Washington State*, Climatic Change, doi: 10.1007/s10584-010-9855-0

Laramie, R.L., and J.C. Schaake, Jr. (1972) *Simulation of the continuous snowmelt process*. In Ralph M. Parsons Laboratory Report Number 143. Massachusetts Institute of Technology: Cambridge.

Legates, DR and T. L. deLiberty (1993) Precipitation measurement biases in the United States. Water Resour. Bull, 29, 855–861.

Liang, X., D. P. Lettenmaier, E. F. Wood, and S. J. Burges (1994) A simple hydrologically based model of land surface water and energy fluxes for general circulation models. J. Geophys. Res, 99, 14,415-14,428.

Linsley, R. L. (1982) Rainfall-Runoff Models ñ An Overview, In: Rainfall-Runoff Relationship, Proceedings of the International Symposium on Rainfall-Runoff Modeling, May 18-21, p. 3-22.

Matheussen, B., R. L. Kirschbaum, I. A. Goodman, G. M. O'Donnell, and D. P. Lettenmaier (2000) Effects of land cover change on streamflow in the interior Columbia River basin (USA and Canada). Hydrol. Processes, 14:867–885.

Palmer, R.N., and M.A. Hahn (2002) The Impacts of Climate Change on Portland's Water Supply: An Investigation of Potential Hydrologic and Management Impacts on the Bull Run System. Report prepared for the Portland Water Bureau, University of Washington, Seattle.

Storck, P. (2000) Trees, snow, and flooding: An investigation of forest canopy effects on snow accumulation and melt at the plot and watershed scales in the Pacific Northwest. PhD dissertation. U. Washington: Seattle; 169.

Storck, P., and D.P. Lettenmaier (1999) *Predicting the effect of a forest canopy on ground snow accumulation and ablation in maritime climates*. In Proc. 67th Western Snow Conf., C. Troendle (ed.). Colorado State U.: Fort Collins: 1 – 12.

Storck, P., L. Bowling, P. Weatherbee, and D.P. Lettenmaier (1998) Application of a GIS based distributed hydrology model for prediction of forest harvest effects on peak stream flow in the Pacific Northwest. Hydrological Processes. 12: 889 – 904.

VanShaar, J.R, I. Haddeland, D. P. Lettenmaier (2002) Effects of land-cover changes on the hydrological response of interior Columbia River basin forested catchments**,** Hydrological Processes, 16 (13) : 2499-2520

Whitaker, A., Y. Alila, J. Beckers, and D. Toews (2003) Application of the Distributed Hydrology Soil Vegetation Model to Redfish Creek, British Columbia: Model evaluation using internal catchment data, Hydrological. Processes. 17, 199-224.

Wigmosta, M.S. and W.A. Perkins (2001) *Simulating the effects of forest roads on watershed hydrology.* In Land Use and Watersheds: Human Influence on Hydrology and Geomorphology in Urban and Forest Areas, M.S. Wigmosta and S.J. Burges (eds.). *AGU Water Science and Application* 2: 127 – 143.

Wigmosta, M.S., B. Nijssen, P. Storck, and D.P. Lettenmaier (2002) *The Distributed Hydrology Soil Vegetation Model*. In Mathematical Models of Small Watershed Hydrology and Applications, V. Singh and D.K. Frevert Water Resource Publications: Highlands Ranch, CO; 7 – 42.

Wigmosta, M.S., L.W. Vail, and D.P. Lettenmaier (1994) *Distributed hydrology vegetation model for complex terrain*. Water. Resources. Res. 30(6): 1665 – 1679